LBL-18841
Preprint

Lawrence Berkeley Laboratory
UNIVERSITY OF CALIFORNIA

Materials & Molecular Research Division

RECEIVED
LAWRENCE
BERKELEY LABORATORY
SEP 9 1985
LIBRARY AND
DOCUMENTS SECTION

Submitted to Physical Review A

BROADBAND AND ADIABATIC INVERSION OF A
TWO LEVEL SYSTEM BY PHASE MODULATED PULSES

J. Baum, R. Tycko and A. Pines

December 1984

TWO-WEEK LOAN COPY
This is a Library Circulating Copy
which may be borrowed for two weeks.

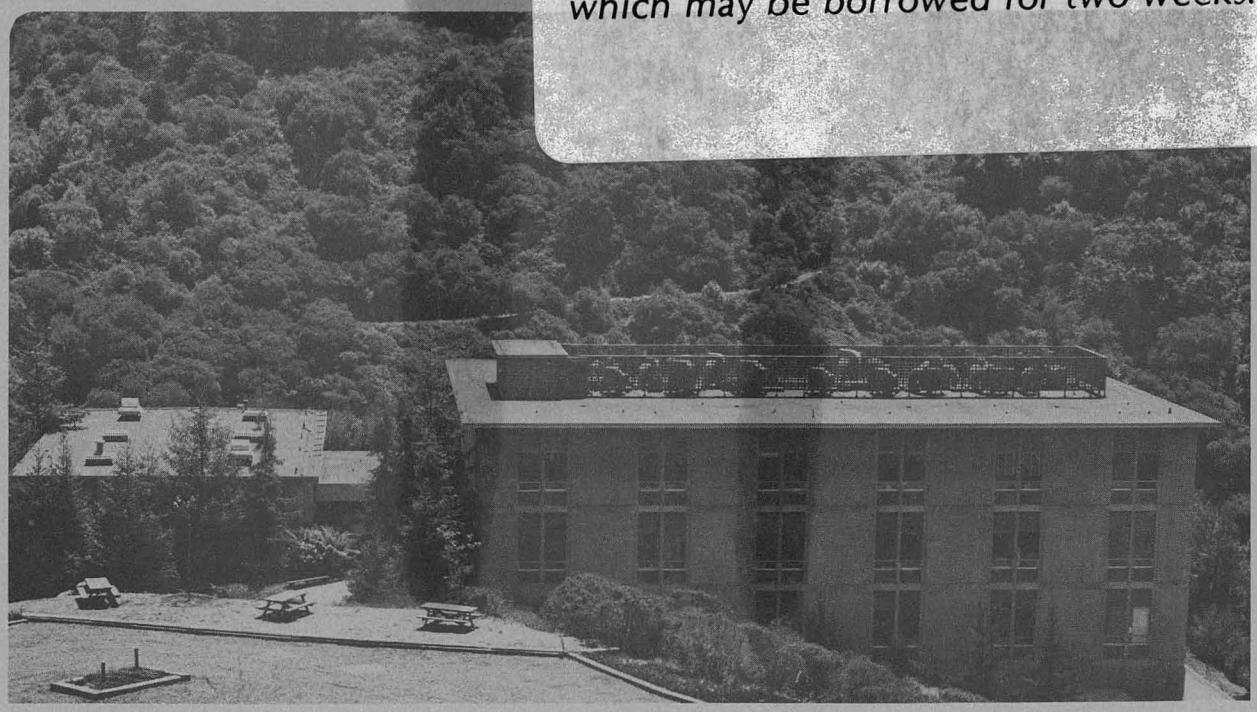

Prepared for the U.S. Department of Energy under Contract DE-AC03-76SF00098

LBL-18841 c.2

DISCLAIMER

This document was prepared as an account of work sponsored by the United States Government. While this document is believed to contain correct information, neither the United States Government nor any agency thereof, nor the Regents of the University of California, nor any of their employees, makes any warranty, express or implied, or assumes any legal responsibility for the accuracy, completeness, or usefulness of any information, apparatus, product, or process disclosed, or represents that its use would not infringe privately owned rights. Reference herein to any specific commercial product, process, or service by its trade name, trademark, manufacturer, or otherwise, does not necessarily constitute or imply its endorsement, recommendation, or favoring by the United States Government or any agency thereof, or the Regents of the University of California. The views and opinions of authors expressed herein do not necessarily state or reflect those of the United States Government or any agency thereof or the Regents of the University of California.

LBL - 18841

BROADBAND AND ADIABATIC INVERSION OF A TWO LEVEL SYSTEM BY PHASE MODULATED PULSES

J. Baum, R. Tycko* and A. Pines

Department of Chemistry, University of California, Berkeley and

Materials and Molecular Research Division, Lawrence Berkeley Laboratory,

Berkeley, CA 94720

* Current address: Department of Chemistry, University of Pennsylvania, Philadelphia, PA 19104

Abstract

We describe a class of continuously phase modulated radiation pulses that result in coherent population inversion on resonance as well as over a large range of transition frequencies and radiation field strengths. This is a population inversion analogy to Self Induced Transparency. Simulations of the inversion properties of the modulated inversion pulse (MIP) are presented. It is shown that the inversion behavior can be explained by treating the MIP as a highly efficient adiabatic sweep. Criteria for establishing adiabaticity are discussed in detail. Finally, a method is presented for generating a sequence of phase shifted radio frequency pulses, from the continously modulated pulse, which can be implemented on modern NMR and coherent optical spectrometers; experimental confirmation is given.

I. INTRODUCTION

A. Background

The implementation of population inversion amongst energy states is an important requirement of many techniques in nuclear magnetic resonance (NMR) and coherent optical spectroscopy, including relaxation time[1] measurements, spin or photon echoes[2,3] and spin decoupling[4]. The simplest way to coherently invert populations is with a single π pulse, i.e. a pulse of radiation such that the product of amplitude in angular frequency units and the time in seconds equals π. For good population inversion to be achieved, the difference between the radiation frequency and the resonant frequency of the transition for which the populations are to be inverted must be much smaller than the radiation amplitude. In other words, the inversion bandwidth of a single π pulse is quite limited. Often it is the case experimentally that the bandwidth of resonant frequencies is comparable to or greater than the available radiation amplitude. In NMR, the bandwidth may result from static magnetic field gradients, chemical shifts or spin couplings. In coherent optics, this may be due to inhomogeneous broadening from crystal strains or Doppler shifts.

An established technique in NMR for inverting spin populations over a large bandwidth is Adiabatic Rapid Passage [5], in which the frequency of applied radio frequency (rf) radiation is swept through the resonances at a constant rate that is small compared to the rf amplitude but large compared to the inverse of the relaxation times. Adiabatic sweeps have been employed in coherent optics as well[6-11]. An alternative approach to broadband inversion in NMR was proposed some time ago by Levitt and Freeman[12]. They suggested using a sequence of phase-shifted pulses, collectively called a compostie π pulse, to produce inversion over a broad

bandwidth. Composite pulses have led to a wide range of applications. Several approaches to their design in NMR[4,12-27] and coherent optics[28-29] have been described. The original work was based on computer simulations of spin trajectories and geometrical intuition[13]. This was followed by a more formal analysis in terms of rotation operators[14-16]. More recent developments include an approach based on coherent averaging theory[17,18] and the introduction of iterative methods for generating composite π pulses[4,19-22]. The coherent averaging theory approach and another approach based on a fictitious spin-1/2 formalism have led to composite pulses for coupled spin systems[23-25].

This paper enlarges upon a recent communication[26] in which we introduced an approach to broadband population inversion that bridges between adiabatic sweeps and composite π pulses. This work -- which was subsequently appreciated by Silver, Joseph, and Hoult[27]-- was originally motivated by the self-induced transparency effect[30] observed in coherent optical spectroscopy. The phenomenon of self-induced transparency, first discovered and studied by McCall and Hahn, occurs when a radiation pulse with an area of 2π and amplitude modulated according to a hyperbolic secant function brings a two-level absorbing system from its ground state back to its ground state regardless of its resonance frequency. In that sense, a hyperbolic secant pulse is a perfectly broadband 2π pulse. Allen and Eberly have proposed a similar class of pulses for population inversion, but with both phase and amplitude modulation[31]. If $\omega_1(t)$ is the amplitude and $\phi(t)$ is the phase of the radiation, the pulse of Allen and Eberly may be written:

$$\omega_1(t) = (\omega_1^0/\sin\gamma)\,\mathrm{sech}(\omega_1^0 t) \qquad (1)$$

$$\dot{\phi}(t) = (\omega_1^0 \cot\gamma)\tanh(\omega_1^0 t) \qquad (2)$$

where t extends from $-\infty$ to $+\infty$. γ is a parameter that determines the depth of the modulation, with no phase modulation when γ equals $\pi/2$ and increasing phase modulation as γ approaches zero. This pulse inverts populations in a two-level system regardless of the values of γ and ω_1^0, provided that the radiation frequency exactly equals the resonance frequency, i.e. "on resonance". Allen and Eberly point out that the pulse resembles an adiabatic sweep for small values of γ, due to the equivalence of phase modulation and frequency modulation. Thus, it may be anticipated that a pulse with phase modulation similar to that of Equation (2) will have broadband inversion properties. The performance of a class of phase modulated pulses related to Eqs. (1) and (2) is investigated in detail below. Comparisons with adiabatic sweeps are made.

The relation to a composite π pulse arises from considering a composite π pulse as a single phase-modulated pulse, with a piecewise-constant phase function. A composite π pulse may then be regarded as an approximation of a continously phase-modulated pulse. One way to generate composite π pulses would be by approximating the continously varying phase function of a pulse similar to that of Equations (1) and (2) by a piecewise-constant function. Procedures for generating composite π pulses from continously phase modulated pulses are developed below.

B. Organization

In Section II, the class of phase-modulated, constant-amplitude pulses first presented in reference 26 is derived from consideration of the

magnetization trajectory. Simulations of population inversion performance are given. A general transformation from a pulse with a modulated phase and a constant amplitude to a pulse with both phase and amplitude modulation is introduced, in order to demonstrate the relationship between our pulses and those of Allen and Eberly.

Section III treats phase-modulated pulses as adiabatic frequency sweeps. Criteria for adiabatic inversion are discussed. They lead to the concept of the efficiency of an adiabatic sweep and to the derivation of a new class of phase-modulated pulses based on efficiency considerations. A comparison of the inversion performance of linear sweeps, pulses derived in Section II, and pulses derived from considerations of efficiency is made.

The treatment of adiabaticity in Section III suggests that the phase modulated pulses of Section II may invert spin populations over large ranges of rf amplitude as well as large ranges of resonant frequencies. The inversion performance as a function of the rf amplitude is treated in Section IV. Section V describes a method for deriving discrete composite pulse sequences from continously phase-modulated pulses. Experimental results are presented.

II. DERIVATION OF PHASE MODULATED PULSES FOR POPULATION INVERSION

A. Frames of Reference

We begin with a description of two frames of reference, shown in Figure 1, that are of importance in the remainder of the paper. The first of these is the usual rotating frame[32]. If an isolated spin or two level system with resonance frequency ω_0 is irradiated with an rf pulse with any general amplitude and phase modulation, its motion in the usual rotating frame is determined by the Hamiltonian H^{PM} (where PM refers to <u>Phase</u>

Modulation):

$$H^{PM} = \Delta\omega I_z - \omega_1(t)[I_x\cos\phi(t) - I_y\sin\phi(t)] \qquad (3)$$

$\omega_1(t)$ and $\phi(t)$ are the pulse amplitude and phase; $\Delta\omega$ is the difference between ω_0 and the rf carrier frequency ω, i.e. the resonance offset. H^{PM} is derived from the laboratory frame Hamiltonian by the transformation T^{PM}:

$$T^{PM} = \exp(-i\omega I_z t) \qquad (4)$$

In this reference frame, which we call the PM frame, the rf frequency appears constant and the phase, i.e. the direction in the xy plane, varies. This is seen in Figure 1a.

An alternate rotating frame transformation that is useful in dealing with continously modulated pulses is accomplished by the unitary operator T^{FM} (where FM refers to Frequency Modulation):

$$T^{FM} = \exp[-i(\omega t + \phi(t))I_z] \qquad (5)$$

In the FM frame, the Hamiltonian is:

$$H^{FM} = (\Delta\omega + \dot{\phi}(t))I_z - \omega_1(t)I_x \qquad (6)$$

and the time derivative of the phase function appears as an additional resonance offset with the xy plane component constant in direction, as shown in Figure 1b. That a phase-modulated pulse can be viewed in either

the PM or FM frames is a statement of the equivalence of phase and frequency modulation. Of course, due to the design of a typical pulsed NMR spectrometer with its constant frequency reference, spin evolution is normally observed in the PM frame. For our purposes, the FM frame serves as a useful tool for deriving modulated pulses.

B. Derivation of phase modulation from magnetization trajectories

An isolated spin can be described in the FM frame by a density operator $\rho(t)$ of the following form:

$$\rho(t) = \underset{\sim}{M}(t).\underset{\sim}{I} \tag{7}$$

where $\underset{\sim}{M}(t)$ is a three-vector proportional to the magnetization and $\underset{\sim}{I}$ is a three-vector whose components are the angular momentum operators[33]. With Equation (6), $\underset{\sim}{M}(t)$ satisfies the Bloch equations without relaxation:

$$\frac{d\underset{\sim}{M}}{dt} = (-\omega_1(t),\ 0,\ \dot{\phi}(t) + \Delta\omega) \times \underset{\sim}{M} \tag{8}$$

If the initial condition for $\underset{\sim}{M}$ is known and if $\dot{\phi}(t)$ and $\omega_1(t)$ are given, then Eq. (8) determines the evolution in time of $\underset{\sim}{M}$. For arbitrary $\dot{\phi}(t)$ and $\omega_1(t)$, Eq. (8) can be solved by numerical methods for ordinary differential equations. Alternatively, $\dot{\phi}(t)$ and $\omega_1(t)$ may be approximated by piecewise-constant functions possibly by dividing time into small intervals over which $\dot{\phi}(t)$ and $\omega_1(t)$ are assigned their respective values at the midpoint of each interval. For each interval with constant $\dot{\phi}(t)$, the evolution of $\underset{\sim}{M}$ is simple. $\underset{\sim}{M}$ precesses around the effective field vector with x component $-\omega_1$ and z component $(\dot{\phi} + \Delta\omega)$ at an angular rate equal to $(\omega_1^2 + (\dot{\phi} + \Delta\omega)^2)^{1/2}$. The length of $\underset{\sim}{M}$ is conserved. If $\underset{\sim}{M}$ is

is assumed to have unit length, $\underset{\sim}{M}$ follows a trajectory on a unit sphere. A trajectory of $\underset{\sim}{M}$ from +z to -z corresponds to the inversion of spin state populations.

An important question which now arises is the following: given a trajectory for $\underset{\sim}{M}(t)$, how can we determine the $\dot{\phi}(t)$ and $\omega_1(t)$ which will yield that trajectory? We begin our consideration of this question with a class of trajectories that is of particular importance in the rest of the paper, namely those that follow a great circle from +z to -z in the FM frame, as depicted in Figure 2a. Appendix A presents a formalism for treating other trajectories. A great circle trajectory is of the form:

$$\underset{\sim}{M}(t) = (\cos\gamma \cos\varepsilon, \sin\gamma \cos\varepsilon, -\sin\varepsilon) \tag{9}$$

where γ is a constant azimuthal angle and ε is a polar angle. ε is a function of t that is to be determined. Since the trajectory depends on the resonance offset, we specify that $\Delta\omega = 0$, i.e. that Eq. (9) should hold on resonance. In addition, we initially search for a pulse with a constant amplitude equal to ω_1^0. The general case of amplitude modulation is treated later. Eqs. (8) and (9) lead to:

$$(-\dot{\varepsilon}\cos\gamma\sin\varepsilon, -\dot{\varepsilon}\sin\gamma\sin\varepsilon, -\dot{\varepsilon}\cos\varepsilon)$$

$$= (-\dot{\phi} \sin\gamma\cos\varepsilon, -\omega_1^0\sin\varepsilon + \dot{\phi} \cos\gamma\cos\varepsilon, - \omega_1^0\sin\gamma\cos\varepsilon) \tag{10}$$

which implies:

$$\varepsilon = (\omega_1^0 \sin\gamma)t \tag{11}$$

$$\dot{\phi} = \omega_1^0 \cos\gamma \tan(\omega_1^0 \sin\gamma t) \tag{12}$$

$$-\frac{\pi}{2\omega_1^0 \sin\gamma} < t < \frac{\pi}{2\omega_1^0 \sin\gamma}$$

Eq. (12) dictates a class of phase-modulated pulses that invert spin populations exactly on resonance, since it is derived from the inverting trajectory in Eq. (9). With $\gamma = \pi/2$, the phase is constant, the PM and FM frames coincide, and a standard π pulse is recovered. $\underset{\sim}{M}(t)$ is confined to a plane perpendicular to the plane of the effective field. As γ approaches zero, the phase modulation deepens, the pulse length increases, and the plane of the magnetization trajectory approaches coincidence wtih the plane of the effective field, suggesting adiabatic behavior. Eq. (11) indicates that $\underset{\sim}{M}(t)$ moves with a constant angular velocity along the trajectory of Eq. (9) regardless of the value of γ, provided that ω_1 is constant.

The derivation of the phase modulation has been carried out in the FM frame. Since the PM and FM frames are related by a rotation about z by $\phi(t)$, the trajectory in the PM frame does not follow a great circle but is still an inverting trajectory. This is shown in Figure 2b. To obtain $\phi(t)$, we integrate Eq. (12):

$$\phi(t) = -\cot\gamma \ln[\cos(\omega_1^0 \sin\gamma t)],$$

where:

$$-\frac{\pi}{2\omega_1^0 \sin\gamma} < t < \frac{\pi}{2\omega_1^0 \sin\gamma} \tag{13}$$

$\dot{\phi}(t)$ and $\phi(t)$ are plotted in Figure 3. A pulse specified by Eqs. (12) and (13) will be referred to as a Modulated Inversion Pulse (MIP). The magnetization trajectory in the PM frame (Figure 2b) is:

$$\begin{aligned} M_x^{PM} &= \cos[\gamma+\phi(t)]\cos((\omega_1^0 \sin\gamma)t) \\ M_y^{PM} &= \sin[\gamma+\phi(t)]\cos((\omega_1^0 \sin\gamma)t) \\ M_z^{PM} &= -\sin((\omega_1^0 \sin\gamma)t) \end{aligned} \tag{14}$$

C. Inversion performance off resonance

Although the MIP is derived so as to invert spin populations on resonance, the appearance of adiabatic behavior suggests that spin populations may be inverted over large ranges of resonance offsets as γ approaches zero. Figure 4 shows simulations of the inversion performance of the MIP as a function of the resonance offset for several values of γ. The extent of inversion is defined to be the negative of the final z component of $\underset{\sim}{M}$. Apparently, the range of offsets for which the inversion is nearly complete can be made as large as desired by taking γ to be sufficiently small.

D. Transformation to amplitude-modulated pulses

Equation (13) is derived above with the assumption of a constant pulse amplitude. Although there is at most one rf phase function that yields a given magnetization trajectory on resonance with a given constant rf amplitude, there may be an infinite variety of combinations of phase and amplitude functions, if amplitude modulation is allowed. Here we present a method for converting a phase-modulated, constant-amplitude pulse to a pulse with both phase and amplitude modulation that produces the same trajectory on resonance.

The essential idea becomes apparent from considering a single pulse with a constant phase ϕ_0, a constant amplitude ω_1^0, and a length τ. The effect of such a pulse when $\Delta\omega = 0$ is to produce a rotation of $\underset{\sim}{M}$ by an angle $\omega_1^0\tau$ about an axis in the xy plane at an angle ϕ_0 to the x axis. Since it is only the area of the pulse that matters, however, the net effect is unaltered if the pulse amplitude is changed, provided that

the pulse length is also changed so that the pulse area remains equal to $\omega_1^0\tau$. In general, a phase-modulated, constant-amplitude pulse can be approximated to arbitrarily high accuracy by a sequence of many constant-phase, constant-amplitude pulses. In order to transform the overall pulse to some desired amplitude modulation, it is then only necessary to increase or decrease the amplitudes of the individual pulses and correspondingly decrease or increase their lengths. The total pulse area must remain constant. Figure 5 illustrates the procedure.

Mathematically, the amplitude transformation is a distortion of time. In general, suppose a pair of functions $\omega_1(t)$ and $\phi(t)$ produce a certain magnetization trajectory, with:

$$\int_{-\infty}^{\infty} \omega_1(t)dt = A \tag{15}$$

If there is another amplitude function $\bar{\omega}_1(t)$, also with area A, then we implicitly define a time transformation $t' = h(t)$ by the relation:

$$\int_0^{t'} \omega_1(u)du = \int_0^{t} \bar{\omega}(u)du \tag{16}$$

<u>The phase function $\bar{\phi}(t) = \phi(h(t))$, along with the amplitude function $\bar{\omega}_1(t)$, will produce the same magnetization trajectory.</u>

Thus we have arrived at the most general procedure for finding phase and amplitude combinations that produce a desired magnetization trajectory. We first derive a unique constant-amplitude pulse. Then we may transform to any other amplitude function of the same area, with the trajectory uniquely determining the pulse area.

To derive the pulses of Allen and Eberly, we transform the pulses of Eq. (13) to the amplitude function of Eq. (1). The corresponding time transformation is:

$$h(t) = \frac{1}{\omega_1^0 \sin\gamma} \tan^{-1}(\sinh \omega_1^0 t) \tag{17}$$

While the pulses of Eqs. (1) and (2) and of Eq. (12) yield the same on-resonance trajectory, the utility of the pulses lies in their ability to invert spins off resonance. The significant, dimensionless quantity that characterizes off-resonance behavior is the ratio $\Delta\omega/\omega_1$. In simulations, we find that the constant amplitude pulses of Eq. (13) give inversion over a larger range of resonance offsets than the amplitude-modulated pulses of Eqs. (1) and (2). An explanation for this is that $\Delta\omega/\omega_1$ is always at its minimum for the constant amplitude pulses.

III. POPULATION INVERSION BY ADIABATIC SWEEPS

We saw in section II that modulated pulses invert spins perfectly on resonance and also over a large range of frequencies as $\gamma \to 0$. Because the on-resonance magnetization trajectories are suggestive of adiabaticity, we now treat the above pulse in the framework of adiabatic sweeps and compare different adiabatic approaches.

A. Criteria for adiabatic inversion

The Hamiltonian of Eq. (6) can be written:

$$H^{FM} = \underset{\sim}{\omega}_{eff}(t) \cdot \underset{\sim}{I} \tag{18}$$

$$\omega_{eff}(t) = (-\omega_1(t),\ 0,\ \Delta\omega + \dot{\phi}(t)) \tag{19}$$

Spin populations may be inverted adiabatically if $\dot{\phi}(t)$ and $\omega_1(t)$ are such that the direction of $\underset{\sim}{\omega}_{eff}(t)$ moves from -z to +z, or from +z to -z, at a sufficiently slow angular rate. In that case, the magnetization, or spin density operator, is said to follow the effective field $\underset{\sim}{\omega}_{eff}(t)$.

If $\underset{\sim}{\omega}_{eff}(t)$ is written as:

$$\underset{\sim}{\omega}_{eff}(t) = \omega_{eff}(t)(-\cos\theta,\ 0,\ \sin\theta) \tag{20}$$

$$\theta = \tan^{-1}[(\Delta\omega + \dot{\phi}(t))/\omega_1(t)] \tag{21}$$

the two criteria for adiabatic inversion by a pulse between times $-t_0$ and t_0 can be stated as follows:[6,7,26]

1. $\left|\frac{d}{dt}\theta(t)\right| \ll \omega_{eff}$

2. $\theta(\pm t_0) \cong \pm\pi/2$

Criterion 1 states that the effective field must change direction slowly compared to the rate at which $\underset{\sim}{M}^{FM}$ precesses. In order to quantify criterion 1, we define the adiabaticity factor Q(t) according to:

$$Q(t) = \omega_{eff}(t)/[\frac{d}{dt}\theta(t)] \tag{22}$$

The larger the value of Q(t), the more adiabatic the frequency sweep.

In what follows, we consider only sweeps for which ω_1 is constant

and non-zero. Therefore, criterion 2 requires that the sweep begin far below resonance and end far above resonance, such that $\left| \Delta\omega + \dot{\phi}(\pm t_0) \right| \gg \omega_1$.

There are many possible forms for $\dot{\phi}(t)$ that result in adiabatic inversion. We call a sweep efficient if it accomplishes population inversion in a comparatively short time. Different forms of sweeps may have different efficiencies for the following reason. Consider criterion 1. Taking ω_1 to be constant, ω_{eff} is smallest when $\theta = 0$ and $\dot{\phi}(t) = -\Delta\omega$, i.e. when the sweep passes through resonance. It is at this time that criterion 1 is most restrictive so that $\left| \frac{d}{dt} \theta(t) \right|$ must be smallest. When the sweep is far from resonance, $\left| \frac{d}{dt} \theta(t) \right|$ may be larger while still satisfying criterion 1 since ω_{eff} is larger. If $\left| \frac{d}{dt} \theta(t) \right|$ indeed becomes larger far from resonance, criterion 2 may be satisfied for comparatively small values of t_0.

In the remainder of this section, three forms of sweeps are examined in light of the above criteria for adiabaticity. The factors that limit their inversion bandwidths are discussed, and their efficiencies are contrasted.

B. Linear sweep

The simplest and most commonly used frequency sweep is a linear sweep defined by:

$$\dot{\phi}(t) = -kt, \quad -t_0 < t < t_0 \tag{23}$$

where k is the constant sweep rate. Since k is constant, criterion 1 is satisfied for all values of $\Delta\omega$ once k is small enough so that criterion 1 is satisfied at any particular value of $\Delta\omega$. For $\Delta\omega = 0$, a linear sweep has:

$$Q(t) = [(\omega_1^0)^2 + \dot{\phi}(t)^2]^{3/2} / k\omega_1^0 \tag{24}$$

$Q(t)$ has its minimum at $t = 0$, where $Q(0) = (\omega_1^0)^2/k$. Simulations show that the maximum value of k for which populations are inverted adiabatically with $\Delta\omega = 0$ is given approximately by $k_{max} = 0.2(\omega_1^0)^2$. This limit is determined by simulating the effects of linear sweeps with t_0 taken to be very large.

For values of k less than or equal to k_{max}, criterion 1 is satisfied throughout the sweep. With k fixed, the choice of t_0 determines whether criterion 2 is satisfied.

Simulations of inversion as a function of $\Delta\omega/\omega_1^0$ for linear sweeps with $k = 0.2(\omega_1^0)^2$ and various values of t_0 are shown in Figure 6. For the inversion to be essentially complete for $\Delta\omega = 0$, the minimum length of the sweep must be given approximately by $2t_0 = 100\omega_1^0$. Inversion is achieved over a large range of resonant frequencies because criterion 2 is satisfied for a large range of resonant frequencies once it is satisfied for $\Delta\omega = 0$. In other words, $\phi(\pm t_0)$ is only a weak function of $\Delta\omega$ when $|\phi(\pm t_0)| \cong \pi/2$. However it is still criterion 2 that ultimately limits the inversion bandwidth for any given value of t_0.

C. Modulated inversion pulse

When treated as a frequency sweep, the MIP of Eq. (12) and Figure 3.a satisfies criterion 2 for all values of γ and $\Delta\omega$. This is because $\dot{\phi}(t)$ becomes infinite at the beginning and end of the pulse. Thus, it is criterion 1 that determines whether the MIP functions as an adiabatically inverting frequency sweep. Recall that the MIP was derived in Section II

in such a way that the inversion at $\Delta\omega = 0$ is complete regardless of γ. The adiabatic nature of the inversion is therefore expressed not by the inversion at $\Delta\omega = 0$, but rather by the appearance of a large inversion bandwidth as γ decreases.

The adiabaticity factor for the MIP with $\Delta\omega = 0$ is given by:

$$Q(t) = [1 + (\cos\gamma \tan\omega_1^0 \sin\gamma t)]^{3/2}/[\cos\gamma \sin\gamma (1 + \tan^2\omega_1^0 \sin\gamma t)] \tag{25}$$

$Q(t)$ has its minimum at $t = 0$, where $Q(0) = (\cos\gamma \sin\gamma)^{-1}$. Broadband inversion occurs when γ is less than or about equal to 0.20, as was seen in Figure 4. When $\gamma = 0.20$, $Q(0) = 5.1$. This result is consistent with the finding that a linear sweep effectively inverts populations only when the sweep rate k is less than or about equal to $0.2(\omega_1^0)^2$, making the adiabaticity factor for a linear sweep greater than or equal to 5. Thus, the adiabaticity factor appears to be a meaningful quantity for predicting the performance of a frequency sweep. In addition, the agreement of the adiabaticity factors for the MIP and the linear sweep supports the contention that the broadband properties of the MIP are due to the adiabatic nature of the inversion.

A comparison of Figures 4 and 6 reveals that nearly complete inversion is achieved by the MIP in less time than by a linear sweep. The sweeps in Figures 6a, 6b, and 6c require the same total time as the MIP in Figure 4 with $\gamma = 0.20$, $\gamma = 0.10$, and $\gamma = 0.05$, respectively. The inversion results in Figure 4 are generally superior, however. Thus, the MIP is a more efficient frequency sweep. This is because the instantaneous sweep rate, i.e. $\dot{\phi}$ is greater at the beginning and end of the sweep than

at $t = 0$.

The fact that the sweep rate is not constant makes criterion 1 the limiting factor on the inversion bandwidth for the MIP. At resonant frequencies for which the sweep rate is rapid as the sweep passes through resonance, defined by the condition $\dot{\phi}(t) = -\Delta\omega$, criterion 1 is not satisfied and populations are not inverted.

D. Constant adiabacity pulse

A third class of frequency sweeps may be derived by making the restriction that $Q(t)$ be constant when $\Delta\omega = 0$.

$$Q(t) = q \tag{26}$$

Based on the above discussion, such a sweep with $q \cong 5$ is expected to be particularly efficient for adiabatic inversion.

Equation (26) implies:

$$q \frac{d\theta}{dt} = \omega_{eff} \tag{27}$$

In addition, we have:

$$\omega_{eff}\cos\theta = \omega_1^0 \tag{28}$$

$$\omega_{eff}\sin\theta = \dot{\phi} \tag{29}$$

Equations (27) and (28) imply:

$$\sin\theta = \omega_1^0 t/q \tag{30}$$

Equation (29) leads to:

$$\dot{\phi}(t) = -(\omega_1^0)^2 t/[q^2-(\omega_1^0)^2 t^2]^{1/2}, \qquad -q/\omega_1^0 < t < q/\omega_1^0 \qquad (31)$$

Equation (31) defines the desired frequency sweep, which we refer to as the constant adiabaticity pulse (CAP). Integration of Eq. (31) gives the equivalent phase modulation:

$$\phi(t) = -[q^2 - (\omega_1^0)^2 t^2]^{1/2} + q \qquad (32)$$

Note that $\phi(t)$ remains finite, although $\dot{\phi}(t)$ becomes infinite at $t = \pm q/\omega_1^0$.

Figure 7 is a comparison of the frequency and phase modulations of the CAP, the MIP, and the linear sweep. The specific parameters in Figure 7 are chosen so that the adiabaticity factor at $t = 0$ is the same for the three sweeps. For a given minimum adiabaticity factor the CAP requires the least total time of the three sweeps.

The adiabaticity factors as functions of time for the CAP, the MIP, and the linear sweep with $\Delta\omega = 0$ are shown in Figure 8. The adiabaticity factor has its minimum value throughout the sweep for the CAP. The adiabaticity factor for the MIP remains close to its minimum value for a greater portion of the sweep than for a linear sweep.

The inversion performance as a function of $\Delta\omega$ for the CAP with various values of q is shown in Figure 9. The values of q are chosen so that the overall lengths of the sweeps in Figure 9 are the same as those in

Figure 4. The bandwidth of the CAP is limited by criterion 1. A comparison of Figures 4,6, and 9 reveals that the MIP exhibits the best inversion performance for equal sweep lengths.

IV. INVERSION IN AN INHOMOGENIOUS RF FIELD

Although the MIP was derived by considering a particular class of inverting trajectories for a spin on resonance, Sections II and III show that the MIP may invert spin populations over large ranges of resonance frequencies due to its adiabatic characteristics. Adiabatic sweeps may invert populations over large ranges of rf amplitudes as well as resonance frequencies. Therefore, in this section we investigate the inversion performance of the MIP as a function of ω_1. Deviations of ω_1 from its nominal value of ω_1^0 arise experimentally from rf inhomogeneity and from miscalibration of the rf field. In coherent optics, it is the laser beam profile that is the analogous source of amplitude inhomogeneity.

The inversion performance as a function of ω_1 may be anticipated by referring to the criteria for adiabatic inversion discussed in Section III. For the MIP, criterion 2 is automatically satisfied, since $\dot{\phi}(t)$ becomes infinite at $\pm t_0$. Once criterion 1 is satisfied for $\omega_1 = \omega_1^0$, it is satisfied even more strongly for $\omega_1 > \omega_1^0$. Therefore, it is expected that essentially complete inversion may be acheived over a large range of ω_1 when the MIP becomes adiabatic, i.e. for $\gamma < 0.20$.

Figure 10 shows simulations of inversion as a function of ω_1 for the MIP with various values of γ. The above predictions are verified. Figure 11 shows a simulated contour plot of inversion as a function of ω_1 and $\Delta\omega$ simultaneously for the MIP with $\gamma = 0.10$. A large region of essentially complete inversion is apparent.

For comparison, Figure 12 shows the inversion performance of a linear sweep as a function of ω_1. Much smaller bandwidths are achieved with much longer sweeps. For a linear sweep, criterion 1 of Section III is

again satisfied for $\omega_1 > \omega_1^0$ once it is satisfied for $\omega_1 = \omega_1^0$. However, criterion 2 is not automatically satisfied. Rather, $\theta(t_0)$ is a strong function of ω_1 when $|\theta(t_0)| \cong \pi/2$, so that criterion 2 is not met at large ω_1.

V. GENERATION OF DISCRETE COMPOSITE PULSES FROM CONTINOUSLY PHASE MODULATED PULSES

It is often difficult to implement the single continously phase modulated pulse experimentally. Frequently it is more convenient to use a sequence of phase shifted rf pulses forming a composite π pulse. This section describes the method by which we approximate the continuous pulse by discrete pulse sequences that have both unrestricted phases as well as rf phases which occur only as multiples of a specified value.

A. General Method of Approximation using magnetization trajectories

The goal is to arrive at a discrete pulse sequence with inversion properties that are very similar to those of the continuously phase modulated pulse. In the computer simulations described above, the MIP is approximated with a large number of pulses, each with a small flip angle, by extracting the individual pulse phases and flip angles from $\phi(t)$ in Equation (13). This was done by dividing the total time interval into subintervals and assigning a constant phase to each subinterval as shown in Figure 13a. As the number of pulses, or subintervals, increases and the flip angles become smaller, this is an increasingly accurate approximation. However, if the number of pulses is small, i.e. less than 100, this is a poor approximation, particularly for small γ. The spin evolution brought about by the MIP over a subinterval is not the same as that brought about by a constant-phase pulse with a phase equal to $\phi(t)$ at the midpoint of that subinterval. Errors in the magnetization trajectory accumulate from

one subinterval to the next, so that even on-resonance spins are no longer inverted. Clearly, a new approximation method is needed. Our method is based on following the on-resonance magnetization trajectory $\underset{\sim}{M}^{PM}(t)$.

Figure 13b is a schematic representation of the method used. The first step is to approximate the trajectory of the magnetization by choosing points in time along it. We then calculate the constant phase pulses that give the evolution of the magnetization from one point to the next. The result is a sequence of radiofrequency pulses or a composite pulse whose magnetization trajectory and inverting properties are very similar to those generated from the continuous pulse.

B. Pulse sequences with unrestricted phases

For a 2n-1 pulse sequence, we need to choose 2n+1 points on the trajectory $\underset{\sim}{M}(t)$. These points are denoted by $\underset{\sim}{M}_0, \underset{\sim}{M}_1, \ldots, \underset{\sim}{M}_n, \ldots \underset{\sim}{M}_{2n}$. The individual flip angles and phases of the derived pulse sequences are denoted respectively by $\theta_1, \ldots, \theta_{2n-1}$ and $\phi_1, \ldots, \phi_{2n-1}$ where $\theta = \omega_1^0 \tau_i$ and τ_i is the length of the ith rf pulse. We set the first point $\underset{\sim}{M}_0 = +z$ and the last point $\underset{\sim}{M}_{2n} = -z$ to ensure that on resonance spins are always perfectly inverted by the discrete pulse sequence. Then in order to follow the trajectory as closely as possible, as indicated in Figure 13b, more points are selected in the regions where $\underset{\sim}{M}^{PM}(t)$ spirals more. A weighting function, $\phi(t)$, which is itself a function of γ is used to generate a set of times $(t_1, \ldots, t_{2n-1})$ from which the intermediate points $\underset{\sim}{M}_i = \underset{\sim}{M}^{PM}(t_i)$ can be calculated.

More specifically, the intermediate points are calculated as follows. First, we choose a value $t_c < 0$ which represents a cut-off time for $\phi(t)$. The means by which t_c is chosen is discussed below. We evaluate $\phi(t_c)$ and calculate a set of phases $(\phi(t_1), \ldots, \phi(t_n))$ satisfying

$$\phi(t_i) = \phi(t_c)(n-i)/n. \tag{33}$$

Using the set of times $(t_1,\ldots,t_n)$ calculated from the set of phases above, we find $\underset{\sim}{M}_1$ through $\underset{\sim}{M}_n$ by evaluating $\underset{\sim}{M}_i = \underset{\sim}{M}^{PM}(t_i)$. The remaining points are determined by the symmetry of $\underset{\sim}{M}^{PM}(t_i)$; $\underset{\sim}{M}_{2n-i}$ is related to M_i by reflection in the xy plane. Next, we calculate the phases and flip angles of the 2n pulses that move on resonance spins between successive points, i.e. that connect $\underset{\sim}{M}_i$ with $\underset{\sim}{M}_{i+1}$. A sequence of pulses with symmetric phases and flip angles emerges. The central two pulses can be fused into one, since they have the same phase, so that an odd number of pulses results.

The "connect-the-dot" method described above ensures that on-resonance spins are inverted. Moreover, the fact that the intermediate $\underset{\sim}{M}_i$ are chosen according to constant increments in $\phi(t)$ ensures that more points occur where $\phi(t)$ is larger, in other words where $\underset{\sim}{M}^{PM}(t)$ spirals most rapidly. Thus, we achieve a good approximation to the trajectory generated from the MIP and it may be expected that the broadband inversion properties of the MIP will be preserved.

In this method, there are only two parameters which must be computer optimized in order to get the best inversion performance over resonance offset or rf inhomogeneity effects, for a specified number of pulses. These are γ and t_c, the cut-off time on $\phi(t)$. They are optimized according to a best-average criterion. This means that we cycle through different values of γ and t_c within certain restrictions, and find the values for which the average inversion, over a specified bandwidth of offsets or rf values, is a maximum.

Figure 14 illustrates three composite pulse sequences that are optimized for broadband inversion with respect to ω_1. Both simulations and experiments are shown. Inversion results for a single π pulse are plotted as a reference. The inversion performance improves for a larger number of pulses.

C. Composite pulses with constant phase increments

For reasons of experimental convenience, it would be desirable to derive sequences in which rf phases occur as multiples of a constant phase. In looking at the form of the pulse sequences derived earlier, we see that the phases ϕ_2 to ϕ_{2n-1} of the 2n-1 pulse sequence occur in constant increments but that ϕ_1 and ϕ_{2n-1} are arbitrary and hold no relationship to the other phases. Our goal in this section is to devise a method whereby we are able to specify the value of the constant phase increment, as well as make the first and last pulse have a phase that is some multiple of that increment.

In our method, the values of the phases, ϕ_2 to ϕ_{2n-2}, of the derived pulse sequence are determined solely from the constant phase increment used on the weighting function $\phi(t)$. The phase of the ith pulse is calculated from the $(i-1)^{st}$ and i^{th} point on the trajectory, by

$$\phi_i = \tan^{-1} \frac{M_x(t_i) - M_x(t_{i-1})}{M_y(t_{i-1}) - M_y(t_i)} \quad 2 < i < 2n-1 \tag{34}$$

By substituting the values for M_x and M_y of Eq. 14 into the above equation and using the fact $\phi(t_i) = (n-i)\phi_0$ (Eq. 33), we find that

$$\phi_i = i\phi_0 + C \tag{35}$$

where C is constant. This indicates that the times corresponding to constant phase increments in $\phi(t)$ also correspond to points on $\underset{\sim}{M}(t)$ that may be connected by pulses with constant phase increments. Therefore we can specify ϕ_0 to be any constant phase we desire, and for a 2n-1 pulse sequence all the calculated pulses from the trajectory between 2 and 2n-2 will have phases that differ by a multiple of ϕ_0.

To ensure that the first and last pulse also have a phase that is a multiple of ϕ_0 the following procedure is used. Rather that setting $\underset{\sim}{M}_0$ and $\underset{\sim}{M}_{2n}$ at $\pm z$ as before, we now choose $\underset{\sim}{M}_{2n}$ such that the pulse connecting $\underset{\sim}{M}_{2n-1}$ to $\underset{\sim}{M}_{2n}$ have a phase $\phi_{2n-1} = m\phi_0$ where m is an integer. In order to still invert on-resonance spins, we also stipulate that $\underset{\sim}{M}_{2n}$ should remain as close to -z as possible. Therefore, to find the best position for $\underset{\sim}{M}_{2n}$ the flip angle of the last pulse is optimized by setting

$$\theta_{2n-1} = \tan^{-1} \frac{M_x(t_{2n-1})\sin(m\phi_0) - M_y(t_{2n-1})\cos(m\phi_0)}{M_z(t_{2n-1})} \tag{36}$$

$\underset{\sim}{M}_0$ is found from $\underset{\sim}{M}_{2n}$ by symmetry. As before,the composite pulse is found by calculating the phases and flip angles ,which connect all the points $\underset{\sim}{M}_i$.

Note that contrary to before, we no longer optimize t_c and thereby ϕ_0, but rather ϕ_0 is chosen and t_c is found from $\phi(t_c) = n\phi_0$. The only parameter to be varied is γ and once again the best average criterion is used to select the pulse sequence that inverts best over the specified range of frequencies and rf amplitudes.

In Figure 15, we show computer simulations and experimental data of inversion versus resonance offset for pulse sequences generated by the

above method. As expected, when the pulse sequence becomes longer, inversion is achieved over a large range of offsets. The inversion bandwidths are comparable to those achieved by recently developed iterative techniques[21-22].

D. Experimental Methods

All of our experiments were performed on a small $H_2O(\ell)$ sample using a homebuilt spectrometer operating at a proton resonance frequency of 360 MHz. The pulse sequence used in the experiments consists of a composite pulse followed by a delay τ = 100ms, followed by a $\pi/2$ detection pulse. Large static field inhomogeneity causes transverse magnetization to dephase during τ. The ensuing FID is collected and Fourier transformed to give the final spectra. The resulting peak height is used as a measure of inversion. The peak height resulting form a single $\pi/2$ pulse alone is used as a calibration. A correction is made for spin-lattice relaxation during τ.

Experimental tests of composite pulses designed for broadband inversion with respect to ω_1 were performed on resonance. The rf amplitude was varied with an attenuator following the transmitter. The length of the detection pulse was adjusted to maintain a constant flip angle. Rf amplitudes were calibrated as in reference 23. Phase shifts were generated by a digitally controlled phase shifter capable of 360°/256 phase increments, with a 3μs switching time. The switching time required that delays be inserted between individual pulses. These delays do not affect inversion performance on resonance, although off resonance performance may degrade appreciably.

Experimental tests of broadband inversion with respect to the resonance offset required rf phases in 45° increments. This was

accomplished by mixing the outputs of the two quadrature generation circuits in the spectrometer. Each quadrature circuit produces phases in 90° increments. A delay line was inserted between the two circuits, producing a phase difference of 45° between them. The quadrature circuits were driven by a variable IF, allowing the resonance offset to be adjusted. The detection pulse was generated independently and maintained on resonance. All experiments were performed with $\omega_1^0/2\pi$ = 10kHz.

SUMMARY

We have described a general analytical procedure for deriving continously phase modulated pulses that result in coherent population inversion on resonance. In the general case, both the phase and amplitude of the inverting pulse can be modulated continuously. Here, however, we have focussed on a class of constant amplitude, phase modulated pulses characterized by a single parameter γ, the depth of modulation. For small values of γ, when the phase modulation is deepened, the modulated inversion pulse (MIP) inverts spin populations simultaneously over large ranges of resonance frequencies and rf amplitudes.

We have proposed that the inversion behavior can be explained by treating the MIP as an efficient adiabatic sweep. To support this, the simulated inversion performance of the MIP is compared to two other adiabatic sweeps in light of two criteria for adiabatic inversion. One sweep is the commonly cited linear frequency sweep and the other is a constant adiabaticity pulse derived directly from considerations of efficiency for adiabatic inversion. Comparisons indicate that the broadband properties of the MIP are in fact due to the adiabatic nature of the pulse and that for equal sweep length the MIP has superior inversion

properties.

Having established the adiabatic properties of the MIP, we then present a method for generating a sequence of phase shifted rf pulses from the continuously phase modulated pulse. The composite pulses are calculated directly from the magnetization trajectory followed by on resonance spins subjected to the MIP. Selected points are chosen along the inverting trajectory and the corresponding constant phase pulses needed to connect these points are found. The broadband properties of the MIP are retained by the discrete pulse sequences, which can then be implemented on most modern NMR spectrometers. This approach connects modulated transparency and inversion pulses used in optics with composite pulses of NMR.

APPENDIX A

In this appendix we treat the problem of finding rf pulses that cause on-resonance magnetization to follow a given trajectory. The trajectory in the FM frame is defined by a function $\underset{\sim}{M}(\varepsilon)$, where $\underset{\sim}{M}$ is the unit magnetization vector in Eq. (7). In the special case of Eq. (9), ε was a polar angle. In general, ε is simply a variable that parametrizes the trajectory. Here we require that ε lie in a unit interval. We make the restrictions that $\underset{\sim}{M}(\varepsilon)$ be continuous and differentiable. These restrictions are consistent with the physical requirements that the trajectory be smooth and unbroken. A piecewise-differentiable trajectory may be treated by considering each piece separately.

With the rf amplitude constant and equal to ω_1^0, the task is now to determine $\varepsilon(t)$ and $\dot{\phi}(t)$. With the definition:

$$\underset{\sim}{\mu} \equiv \frac{d\underset{\sim}{M}}{d\varepsilon} \tag{A.1}$$

Eq. (8) becomes:

$$\dot{\varepsilon}\underset{\sim}{\mu} = (-\omega_1^0, 0, \dot{\phi}) \times \underset{\sim}{M} \tag{A.2}$$

leading to:

$$\dot{\phi} = \omega_1^0 \frac{\mu_x}{\mu_z} \tag{A.3}$$

$$\dot{\varepsilon} = -\frac{\omega_1^0 M_y}{\mu_z} \tag{A.4}$$

Eq. (A.3) gives the phase modulation as a function of ε. Eq. (A.4) gives t as a function of ε:

$$t = -\int_0^{\varepsilon} d\varepsilon' \frac{\mu_z}{\omega_1^0 M_y} \tag{A.5}$$

Inverting Eq. (A.5) gives ε as a function of t, which completes the derivation of the phase modulation.

The phase function obtained in this way produces the desired trajectory for $\Delta\omega = 0$ and $\omega_1(t) = \omega_1^0$. For non-zero values of $\Delta\omega$, the same trajectory may be produced by subtracting the constant $\Delta\omega$ from $\dot{\phi}$ in Eq. (A.3). Of course, this is equivalent to shifting the rf carrier frequency. The phase function that corresponds to an amplitude modulated pulse can be derived according to the discussion in Section II.D.

Finally, it should be realized that not all trajectories are obtainable. In particular, there is no pulse that produces the desired trajectory if t is not a monotonic function of ε in Eq. (A.5).

ACKNOWLEDGEMENTS

AP acknowledges helpful discussions with E. L. Hahn and J. H. Eberly. This work was supported by the Director, Office of Energy Research, Office of Basic Energy Sciences, Materials Science Division of the U.S. Department of Energy and by the Director's Program Development Funds of the Lawrence Berkeley Laboratory under Contract Number DE-AC03-76SF00098.

References

1. R.L. Vold, J.S. Waugh, M.P. Klein, D.E. Phelps, J. Chem Phys. 48, 3831 (1968).

2. a) H.Y. Carr and E.M. Purcell, Phys. Rev. 94, 630 (1954).
   b) S. Meiboom and D. Gill, Sci. Inst. 29, 688 (1958).
   c) E.L. Hahn, Phys. Rev. 80, 580 (1950).

3. D. Abella, N.A. Kurnit, S.R. Hartmann, Phys. Rev. 141, 391 (1966).

4. M.H. Levitt, R. Freeman, T. Frenkiel, Adv. Magn. Reson. 11, 48 (1983).

5. A. Abragam, "The Principles of Nuclear Magnetism" (Oxford University Press, London, 1961), p. 44.

6. D. Grischkowsky, "Laser Applications to Optics and Spectroscopy", Vol. II of Physics of Quantum Electronics Series edited by S.F. Jacobs, M. Sargent III, J.F. Scott, and M.O. Scully (Addison-Wesley, Reading, Mass. 1975). p. 437.

7. M.D. Crisp, Phys. Rev. A 8, 2128 (1973).

8. M.M.T. Loy, Phys. Rev. Lett. 32, 814 (1974).

9. M.M.T. Loy, Phys. Rev. Lett. 41, 473 (1978).

10. E.B. Treacy, Physics Letter 27A, 421 (1968).

11. E.B. Treacy, J. Demaria, Physics Letters 29A, 369 (1969).

12. M.H. Levitt and R. Freeman, J. Magn. Reson. 33, 473 (1979).

13. R. Freeman, S.P. Kempsell and M.H. Levitt, J. Magn. Reson. 38, 453 (1980).

14. M.H. Levittt and R. Freeman, J. Magn. Reson. 43, 65 (1981).

15. M.H. Levitt, J. Magn. Reson. 48, 234 (1982).

16. M.H. Levitt, J. Magn. Reson. 50, 95 (1982).

17. R. Tycko, Phys. Rev. Lett. 51, 775 (1983).

18. R. Tycko, H.M. Cho, E. Schneider, and A. Pines, J. Magn. Reson. 61, 90 (1985).

19. M.H. Levitt and R.R. Ernst, J. Magn. Reson. 55, 247 (1983).

20. A. J. Shaka and R. Freeman, J. Magn. Reson. 59, 169 (1984).

21. R. Tycko and A. Pines, Chem. Phys. Lett. 111, 462 (1984).

22. R. Tycko, J. Guckenheimer, and A. Pines, J. Chem. Phys., in press.

23. R. Tycko, E. Schneider, and A. Pines, J. Chem Phys. 81, 680 (1984).

24. T.M. Barbara, R. Tycko, D.P. Weitekamp, J. Magn. Reson. 62, 54 (1984).

25. M. Levitt, D. Suter, and R. Ernst, J. Chem Phys. 80, 3064 (1984).

26. J. Baum, R. Tycko, and A. Pines, J. Chem Phys. 79, 4643 (1983).

27. M.S. Silver, R.I. Joseph, and D.I. Hoult, Phys. Rev. A 31, 2753 (1985).

28. W.S. Warren and A.H. Zewail, J. Chem. Phys. 78, 2279 (1983).

29. W.S. Warren, J. Chem. Phys. 81, 5437 (1984).

30. S.L. McCall, E.L. Hahn, Phys. Rev. 183, 457 (1969).

31. L. Allen, J.H. Eberly, "Optical Resonance and Two-Level Atoms" (John Wiley and Sons, New York, 1975).

32. I.I. Rabi, N.F. Ramsey, and J. Schwinger, Rev. Mod. Phys. 26, 167 (1954).

33. R.P. Feyman, F.L. Vernon, R.W Hellwarth, J. Appl. Phys. 28, 49 (1957).

Figure 1

a). Phase modulated (PM) frame

b). Frequency modulated (FM) frame

The resonance offset, $\Delta\omega = \omega_0 - \omega$, is the difference between the Larmor frequency and the rf carrier frequency. The pulse amplitude and phase are denoted by $\omega_1(t)$ and $\phi(t)$, respectively. In the PM frame which is the equivalent of the usual rotating frame used in NMR, the phase of the pulse which varies with time, gives the direction of the radiation in the xy plane. In the FM frame, the direction of the radiation in the xy plane is fixed, and the time derivative of the phase function, $\dot{\phi}(t)$, appears along the z direction as an additional resonance offset. The two frames are related by a rotation about the z axis by $\phi(t)$.

Figure 2

Inverting magnetization trajectories for an on-resonance spin the the FM (a) and PM (b) frames calculated from equations (9,11) and (13,14) respectively, with $\gamma = 0.1$.

Figure 3

Continuously frequency (a) and phase (b) modulated inversion pulse (MIP) plotted versus $\omega_1^0 t$ for values of $\gamma = 0.2$ and $\gamma = 0.1$. The pulse amplitude is constant and the phase modulation increases as γ decreases. Also, as $\gamma \to 0$, the overall pulse length increases ($2\omega_1^0 t = \pi/\sin\gamma$). The MIP is an exact analytical solution to the problem of population inversion on resonance ($\Delta\omega = 0$) for all values of γ.

Figure 4

Simulations of spin inversion from the MIP as a function of the relative resonance offset for various values of γ. Inversion is defined as the negative of the final z component of the spin angular momentum; initially the spin system has a z component of +1. For all values of γ, the inversion is always perfect on resonance. For $\gamma = \pi/2$, i.e. no phase modulation, the MIP is equivalent to a standard π pulse, which can be used here as a reference. As $\gamma \to 0$, i.e. increasing phase modulation, a good inversion is accomplished over an increasingly large range of frequencies.

Figure 5

Schematic representation of the transformation from a pulse with constant amplitude and phase modulation (a) to a pulse with both amplitude and phase modulation (b). In (a) the total time interval is divided into subintervals of length τ, represented by the dashed lines, which are each assigned a constant phase and a flip angle = $\omega_1\tau$. The transformation from (a) to (b) is effected by choosing the desired overall amplitude modulation, and then changing the lengths of the individual pulses while still maintaining that their flip angle remain equal to $\omega_1\tau$. The new phase modulation emerges from the time transformation.

Figure 6

Simulations of inversion as a function of resonance offset, resulting from the linear frequency sweep of Eq. (23) of the text with $k/(\omega_1^0)^2 = 0.2$. The linear sweep consists of a constant amplitude rf field whose frequency is changing at a constant rate of $k/(\omega_1^0)^2$. The overall lengths of the sweeps are $2\omega_1^0 t_0$ = 15.82 (a) 31.46 (b) 62.86 (c) 200.0 (d). The minimum overall

length required to achieve adiabatic inversion on resonance is approximately $2\omega_1^0 t_0 = 100$. Once inversion is achieved on resonance, it is also accomplished over a large range of resonant frequencies. The overall lengths of 6 (a), (b) and (c) are equal to the overall lengths of the sweeps used to simulate inversion performance from the MIP in Figure 4 when $\gamma = 0.20$, 0.10, and 0.05 respectively.

Figure 7

Comparison of 3 adiabatic frequency (a) and phase (b) modulated pulses: the constant adiabatic pulse (CAP), the MIP and the linear sweep. The CAP, a constant amplitude pulse, was derived from considerations of efficiency for adiabatic sweeps. In this figure, the parameters were chosen such that the adiabaticity factor Q(t) defined by Equation 22, be equal to 10.067 for all three pulses at t = 0. The larger the value of Q(t), the more adiabatic the sweep.

Figure 8

Comparison of the adiabaticity factors Q(t) with $\Delta\omega = 0$ for the MIP, the linear sweep and the CAP. Q(t) is defined in the text by Equations (25), (24), and (26) respectively. The efficiency of the sweep is determined by the length of time Q(t) remains close to its minimum; the linear sweep is the least efficient sweep.

Figure 9

Simulations of inversion as a function of $\Delta\omega/\omega_1^0$ for the CAP. The overall lengths of the sweeps were chosen such that they correspond to the overall lengths of the sweeps of Figure 4 ($q = \pi/2\sin\gamma$, the overall length is 2q).

Simulations indicate that when $Q(0) > 5$, the CAP, the MIP and the linear sweep exhibit adiabatic inversion over a large range of frequencies. A comparison of figures 4, 5(a)(b)(c) and 8 indicate that the MIP produces the best adiabatic broadband inversion for equal sweep lengths and always inverts on resonance spins.

Figure 10

Simulations of inversion as a function of ω_1/ω_1^0 for the MIP with values of γ as shown. When $\gamma < 0.2$ ($Q(0) > 5$), the inversion becomes perfect over a very large range of ω_1.

Figure 11

Simulated contour plot of population inversion as a function of $\Delta\omega$ and ω_1 for the MIP with $\gamma = 0.10$. The MIP compensates simultaneously for resonance offset and rf inhomogeneity effects.

Figure 12

Simulated inversion performance as a function of ω_1/ω_1^0 for the linear sweep with $k/(\omega_1^0)^2 = 0.2$. The overall pulse lengths are $2\omega_1^0 t_0 = 31.46$ (a), 62.86 (b), 100.0 (c), 200.0 (d). For longer sweeps that shown in Fig. 10, the inversion is poorer.

Figure 13

a) Schematic diagram of a method for approximating the MIP by a large number of constant phase pulses. The total length of the pulse is divided into a large number of subintervals with lengths inversely proportional to $\dot{\phi}(t)$; this is indicated by the dotted lines. The pulse flip angles are

calculated from the subinterval lengths and the constant amplitude. Based on $\phi(t)$, a constant phase is assigned to each subinterval. If the number of pulses is small, this is a poor approximation.

b) Schematic representation of the method used to approximate the continuously modulated pulse (MIP) by a discrete pulse sequence. The magnetization trajectory $\underset{\sim}{M}^{PM}(t)$ of an on-resonance spin subjected to the MIP is approximated by a discrete number of points. The flip angle and constant phase that give the evolution of the magnetization from one point to the next are calculated. The result of this "connect the dots" technique is a composite pulse whose inversion properties are similar to those of the continuous pulse.

Figure 14

Simulations (solid lines) and ^{1}H experimental measurements (dots) of population inversion as a function of ω_1/ω_1^0 for discrete pulse sequences derived from the MIP using the technique described in Fig. 13b. Results are shown for (a) single π pulse presented as a reference; (b) 3 pulse sequence $(54)_{90}(162.8)_0(54)_{90}$; (c) 31 pulse sequence $(18.3)_{264}(4.8)_{185}(5.3)_{172}(5.7)_{159}(6.3)_{146}(6.9)_{132}(7.6)_{119}(8.5)_{106}(9.4)_{93}(10.6)_{79}$ $(12.0)_{66}(13.9)_{53}(16.4)_{40}(20.2)_{26}(27.3)_{13}(127.0)_0(27.3)_{13}(20.2)_{26}(16.4)_{40}$ $(13.9)_{53}(12.0)_{66}(10.6)_{79}(9.4)_{93}(8.5)_{106}(7.6)_{119}(6.9)_{132}(6.3)_{146}(5.7)_{159}$ $(5.3)_{172}(4.8)_{185}(18.3)_{264}$. The notation is $(\theta)_\phi$ where θ and ϕ are the flip angles and phases of individual pulses in degrees.

Figure 15

Simulations (solid lines) and ^{1}H experimental measurements (dots) of population inversion as a function of $\Delta\omega/\omega_1$ for discrete pulse sequences

derived from the MIP. Results are shown for (a) single π pulse presented as a reference; (b) 7 pulse sequence $(39.6)_{315}(68.4)_{180}(87.9)_{90}(275.7)_{0}$ $(87.9)_{90}(68.4)_{180}(39.6)_{315}$; (c) 11 pulse sequence $(30.2)_{270}(28.7)_{180}(34.9)_{135}$ $(43.8)_{90}(58.9)_{45}$ $(225.4)_{0}(58.9)_{45}(43.8)_{90}(34.9)_{135}(28.7)_{180}(30.2)_{270}$; (d) 15 pulse sequence $(21.5)_{0}(19.4)_{270}(23.0)_{225}(27.5)_{180}(33.6)_{135}(42.5)_{90}$ $(57.5)_{45}(222.8)_{0}(57.5)_{45}(42.5)_{90}(33.6)_{135}(27.5)_{180}(23.0)_{225}(19.4)_{270}(21.5)_{0}$.

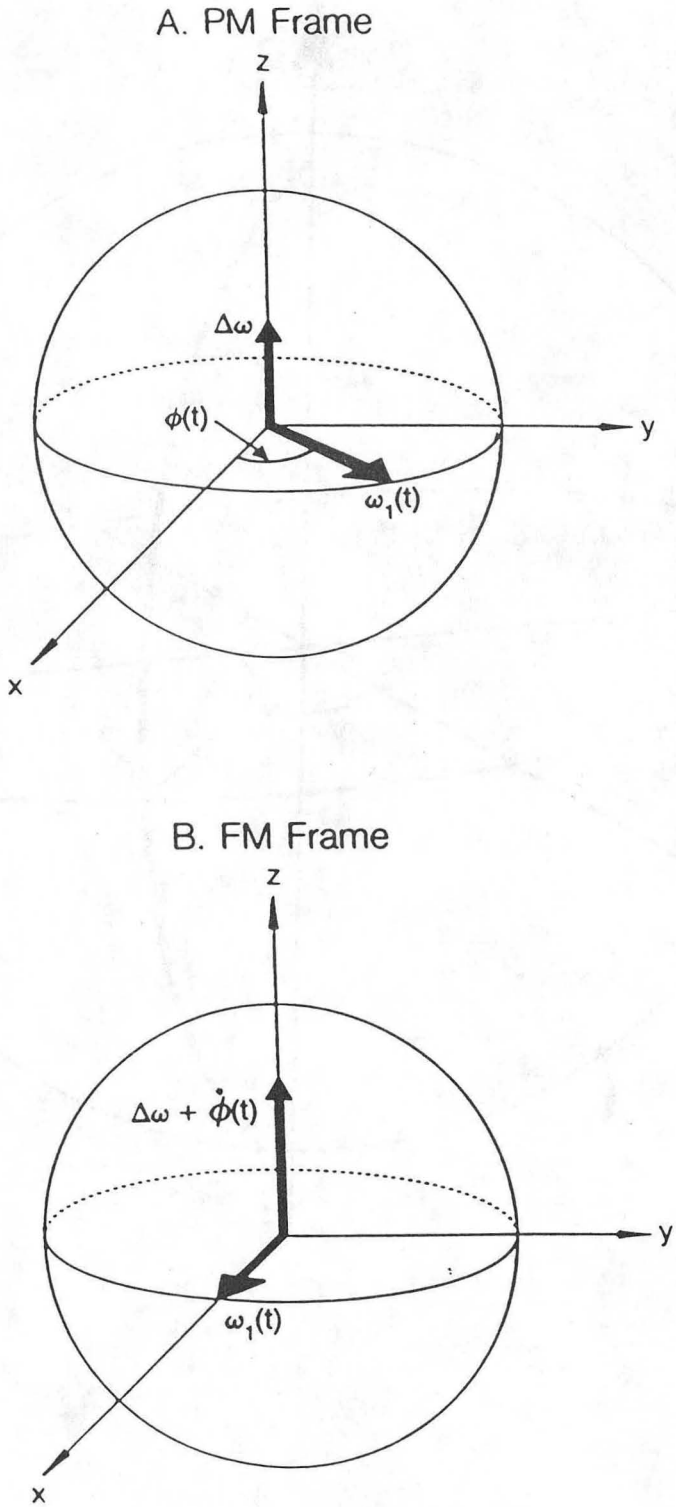

XBL 855-8870

Figure 1

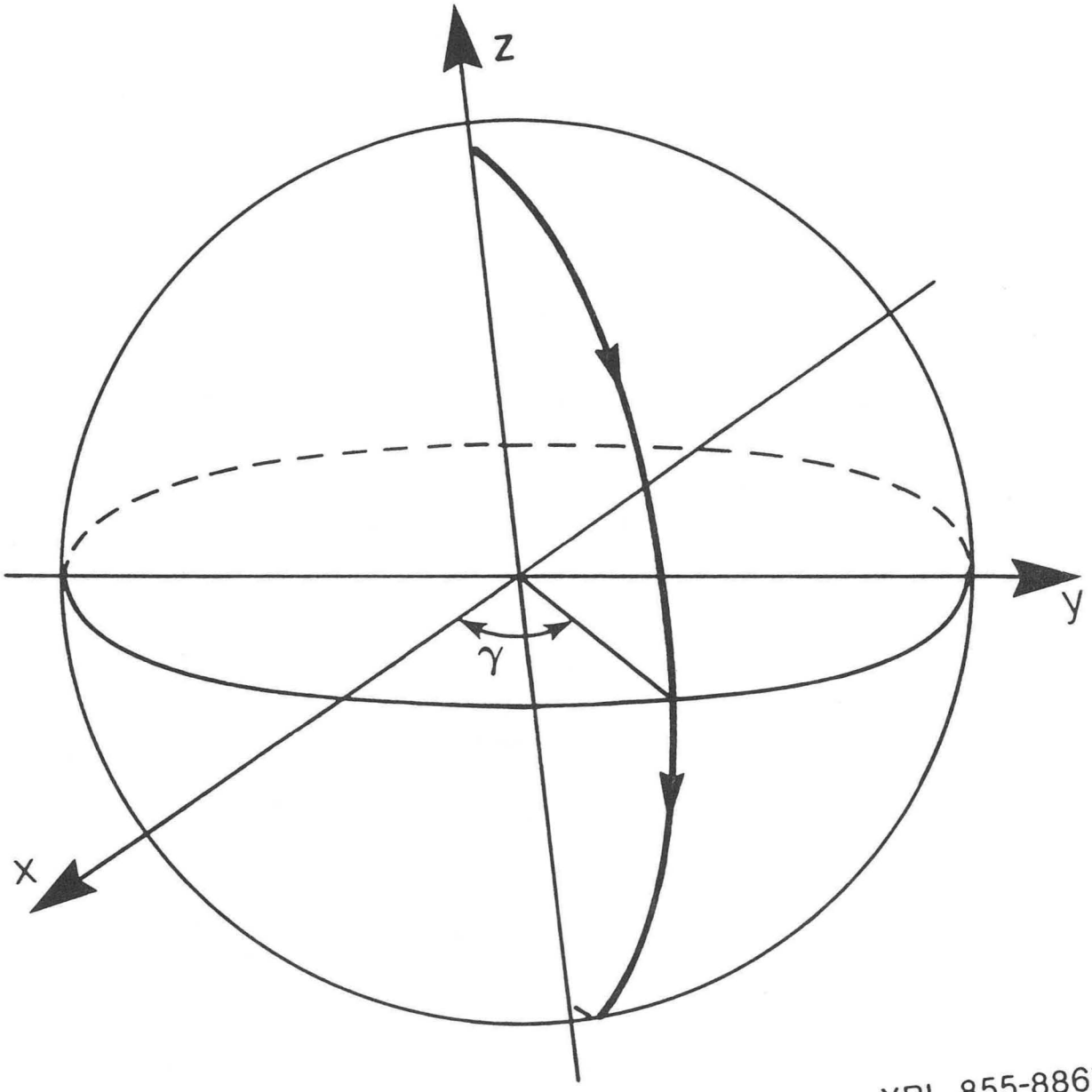

XBL 855-8867A

Figure 2a

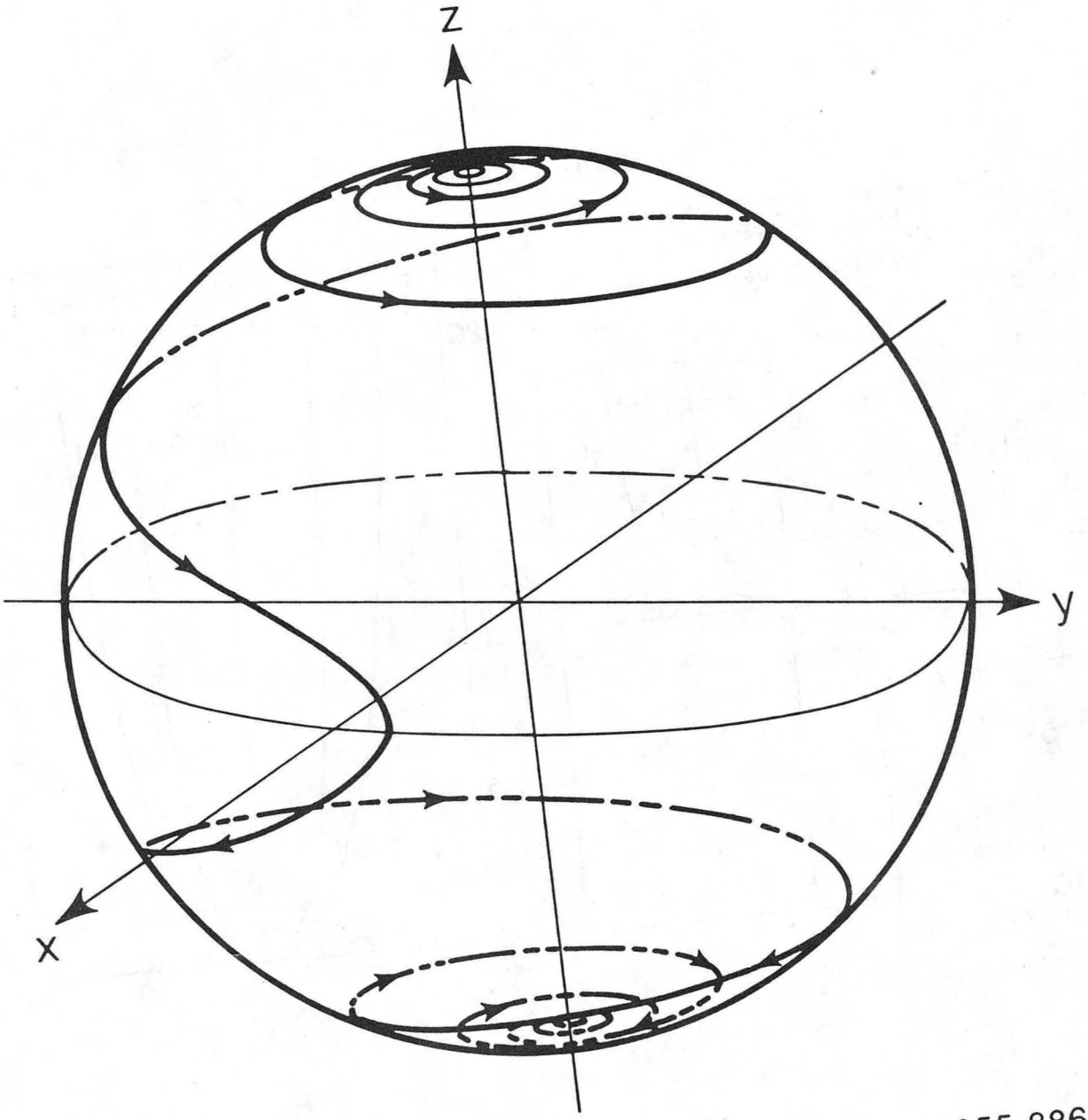

XBL 855-8869A

Figure 2b

MODULATED INVERSION PULSE

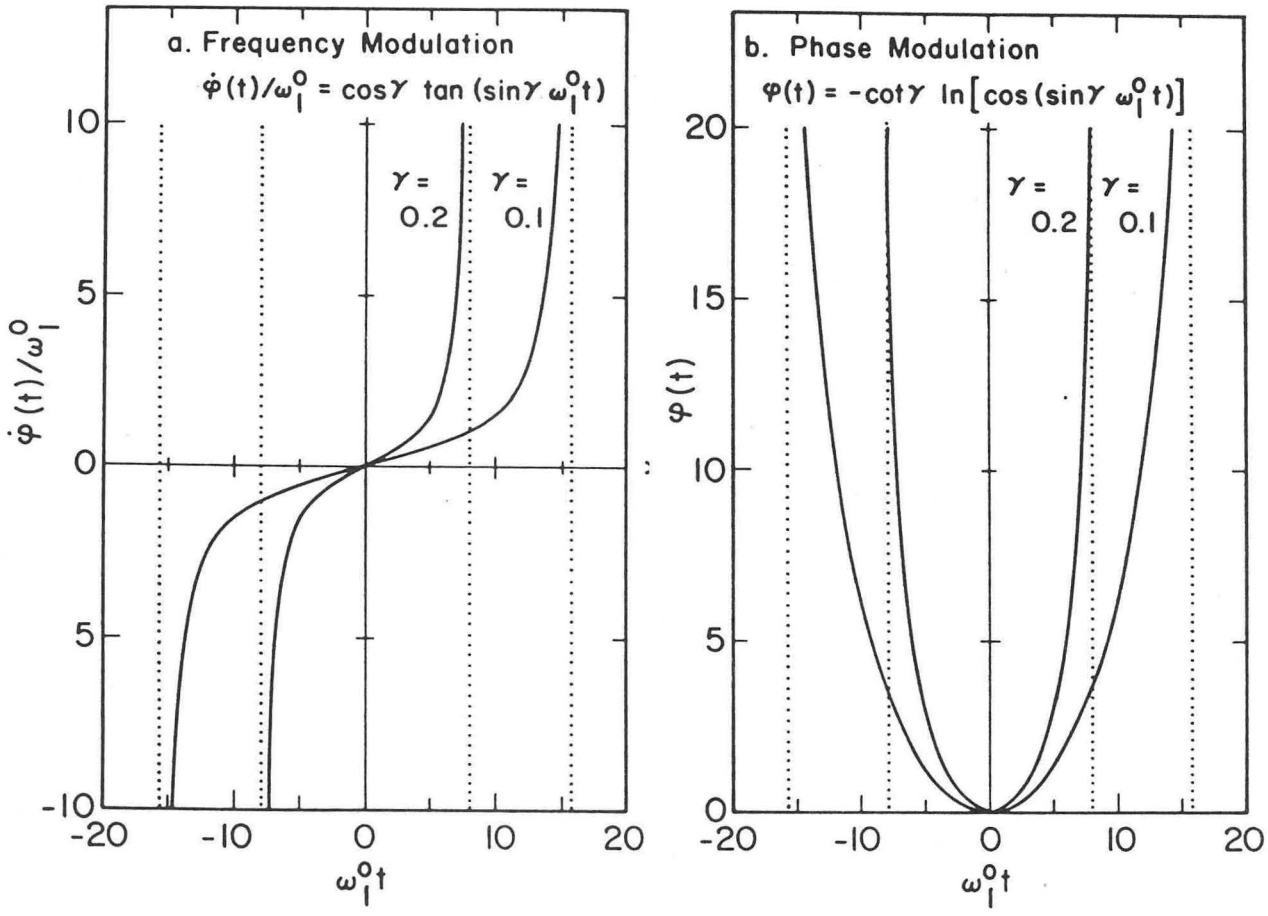

XBL 855-2605

Figure 3

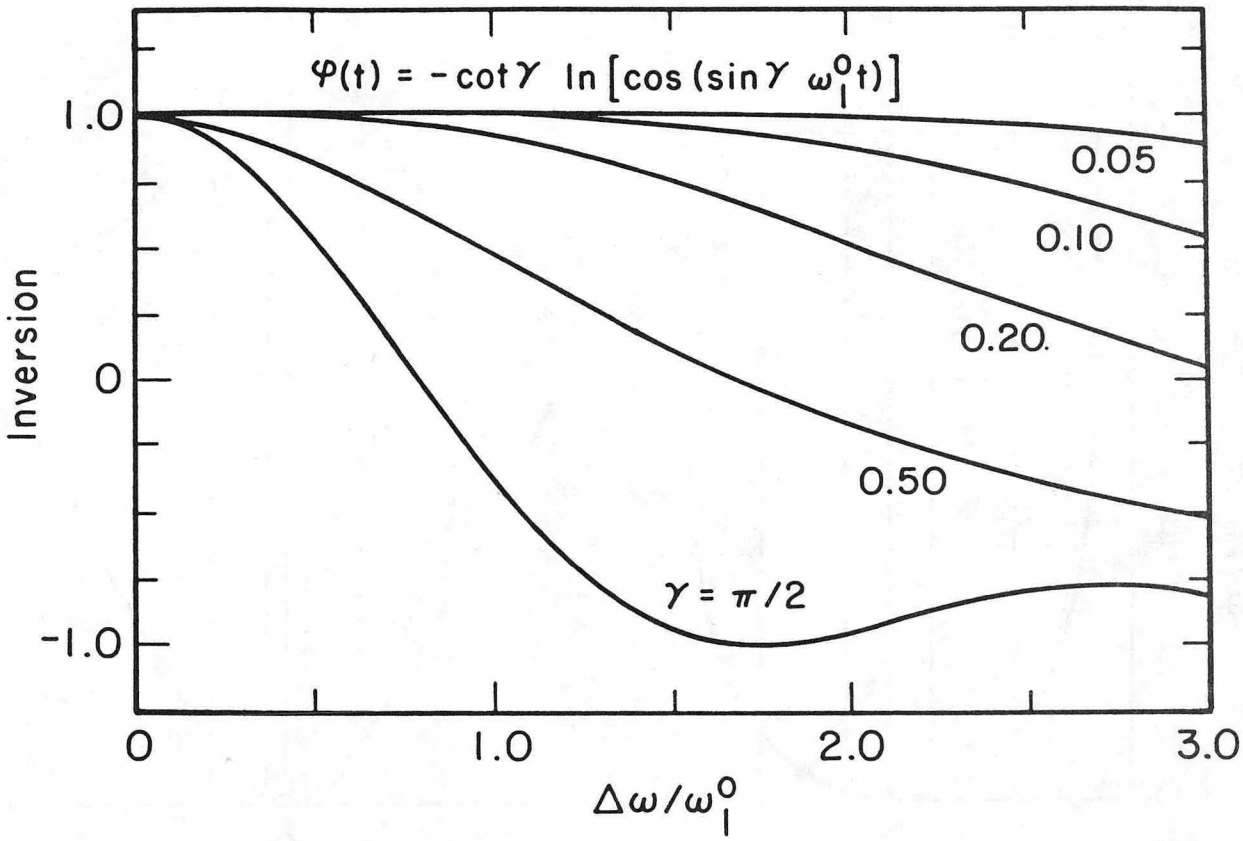

XBL 855-2601

Figure 4

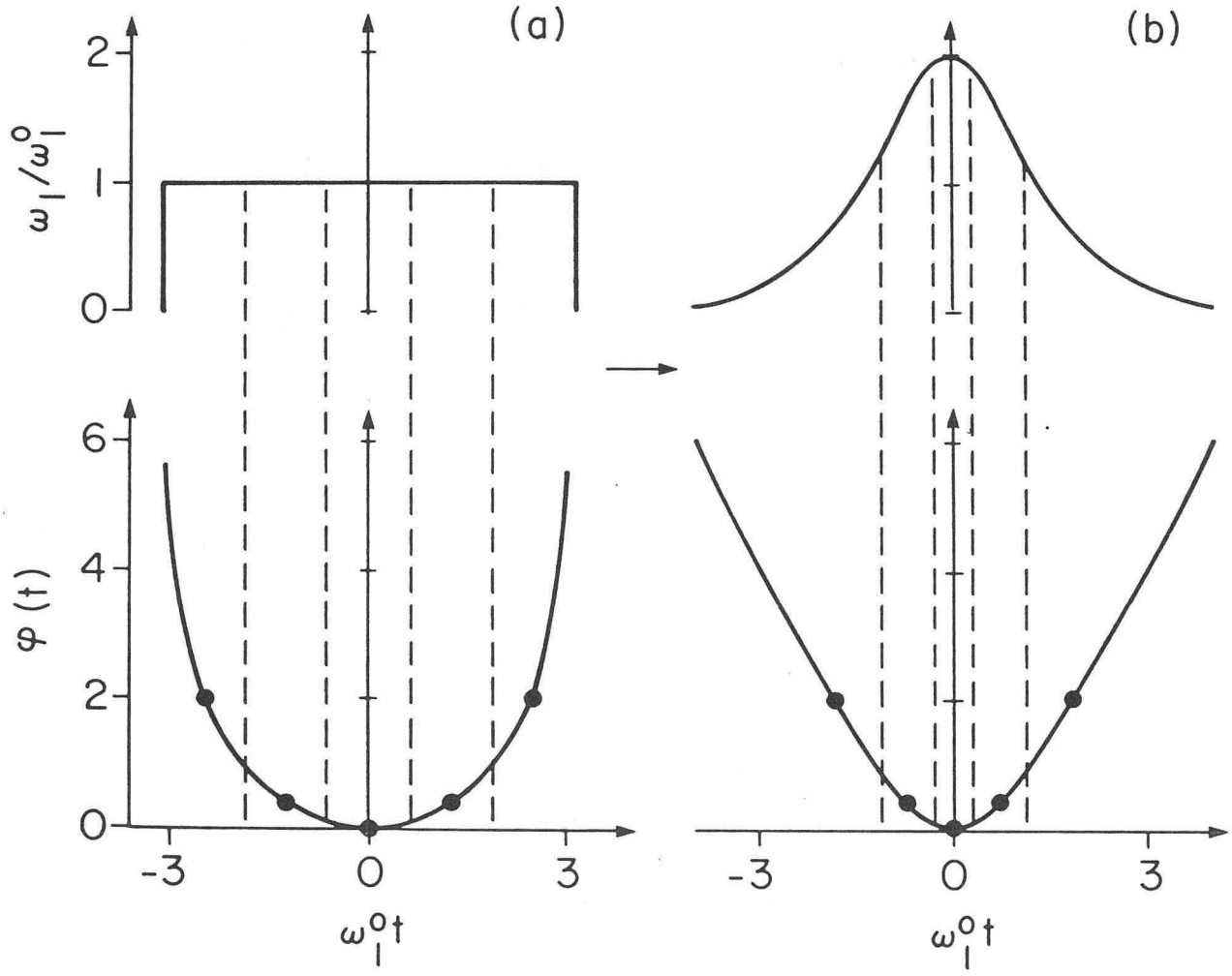

XBL 855-2604

Figure 5

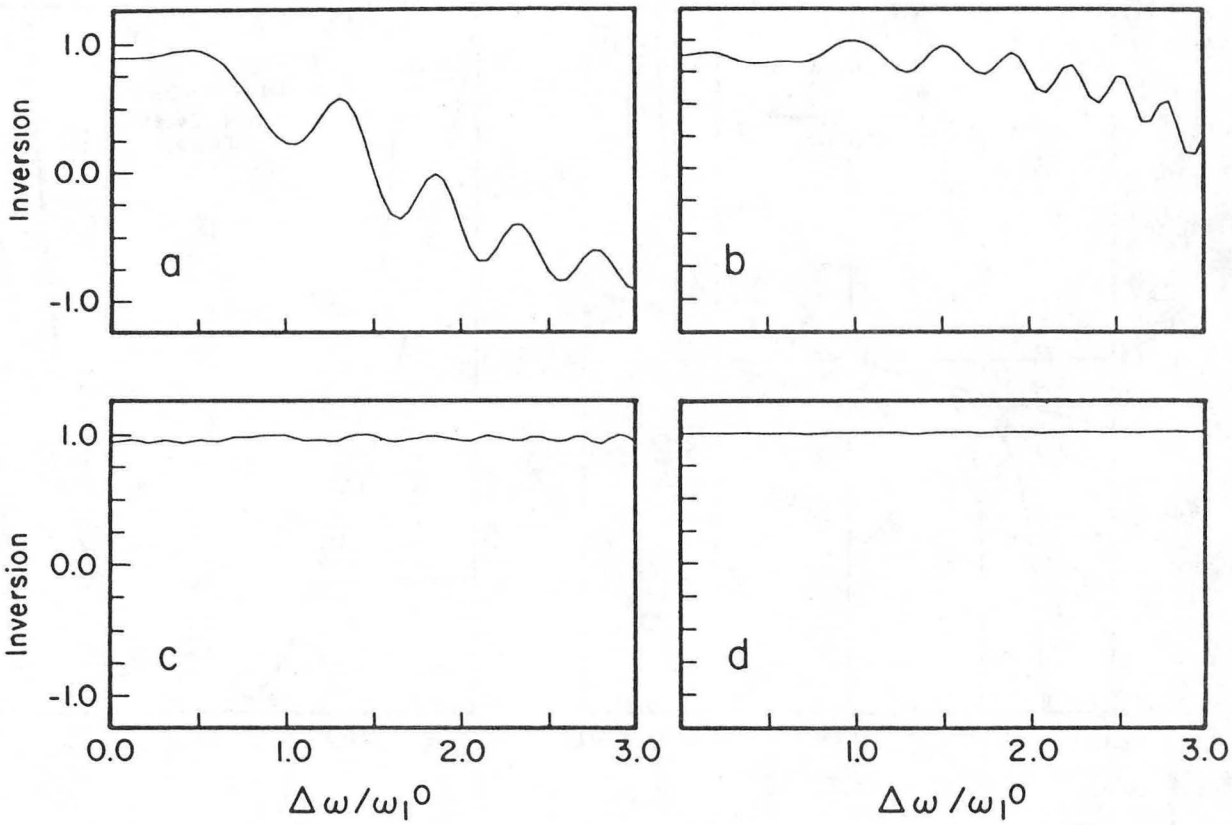

XBL 855-2602

Figure 6

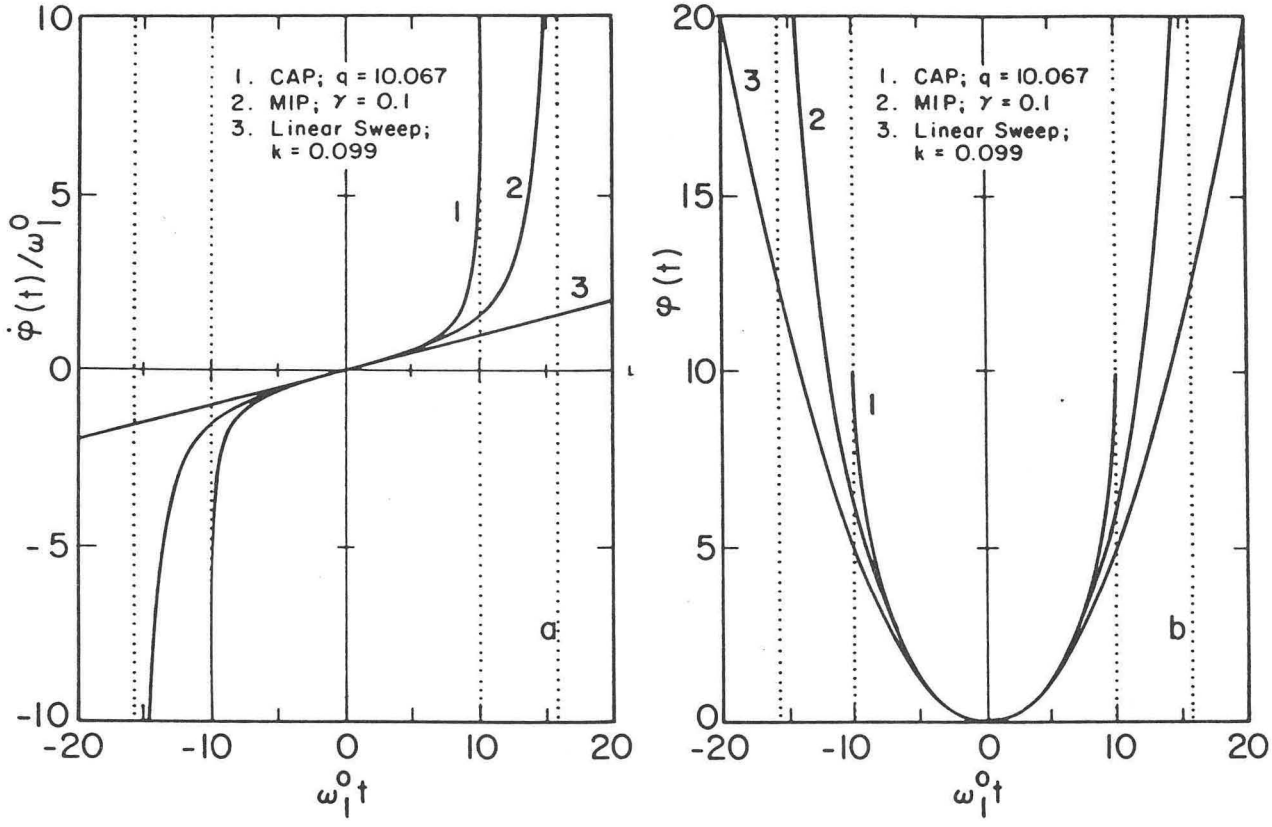

XBL 855-2614

Figure 7

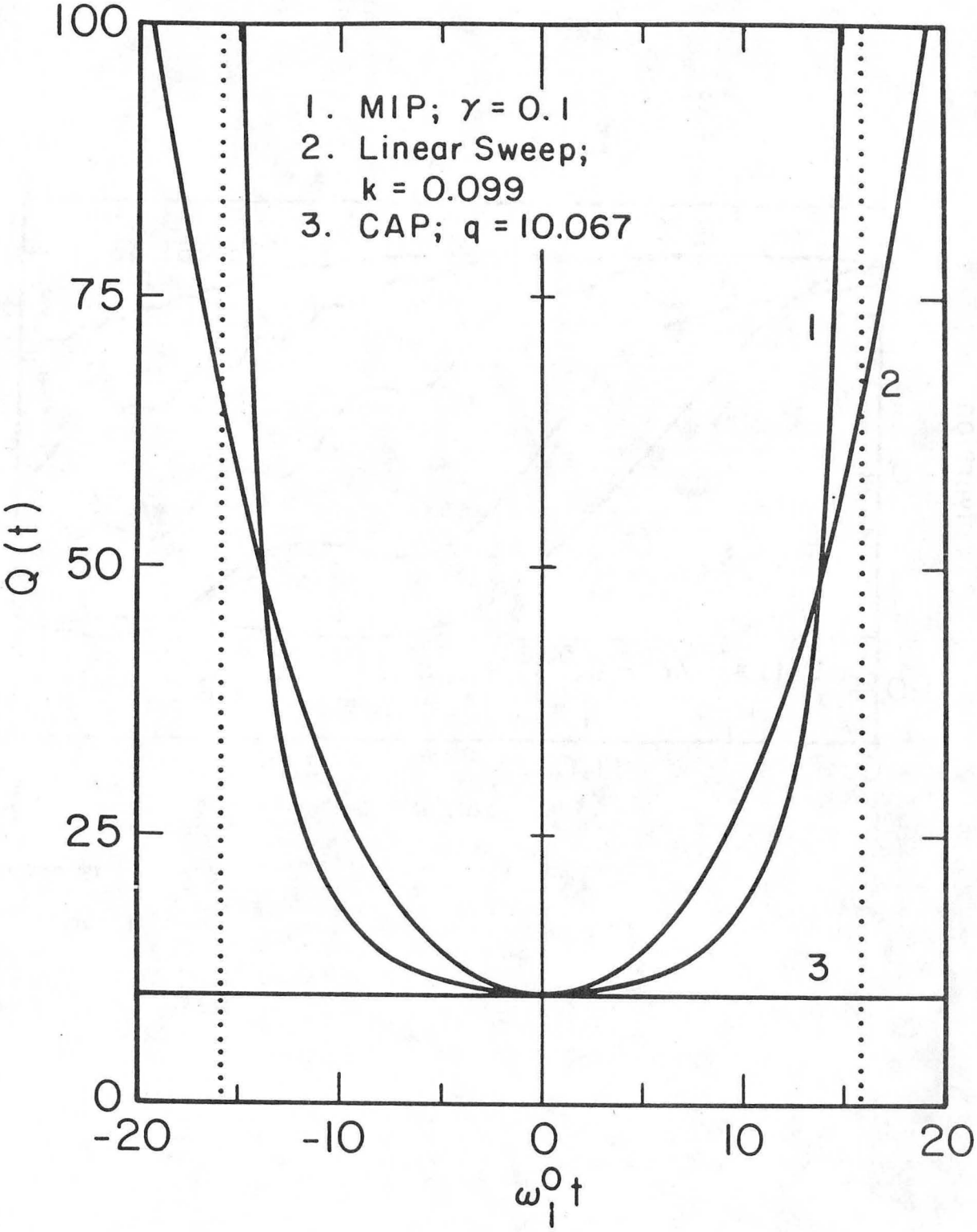

XBL 855-2610

Figure 8

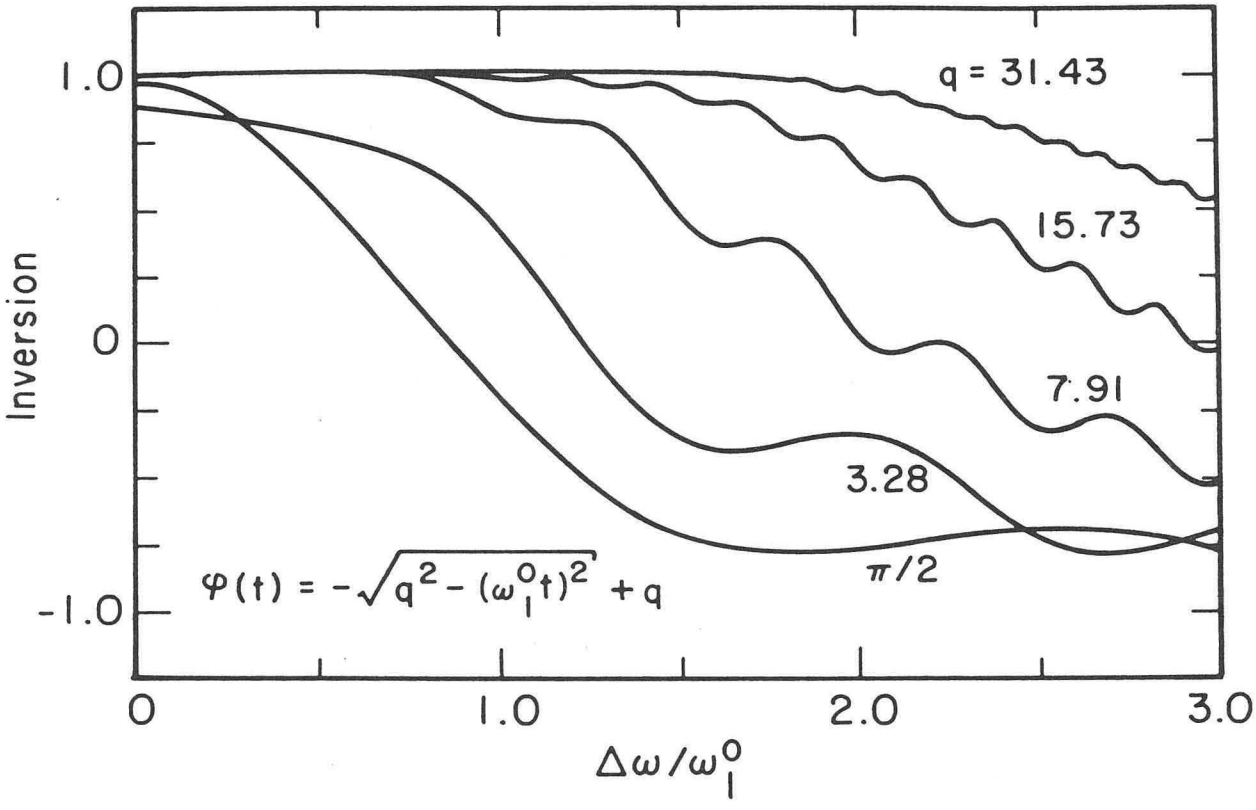

XBL 855-2609

Figure 9

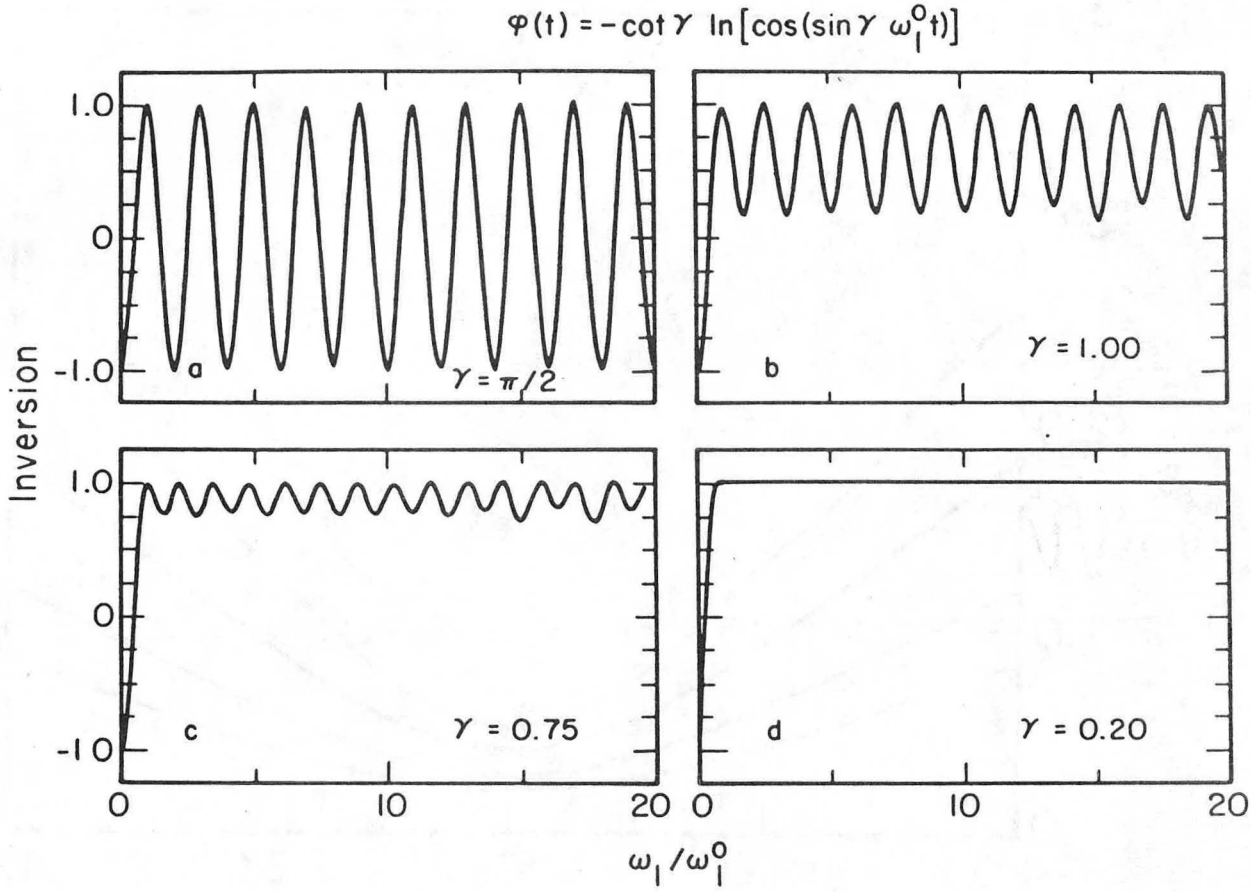

XBL 855-2608

Figure 10

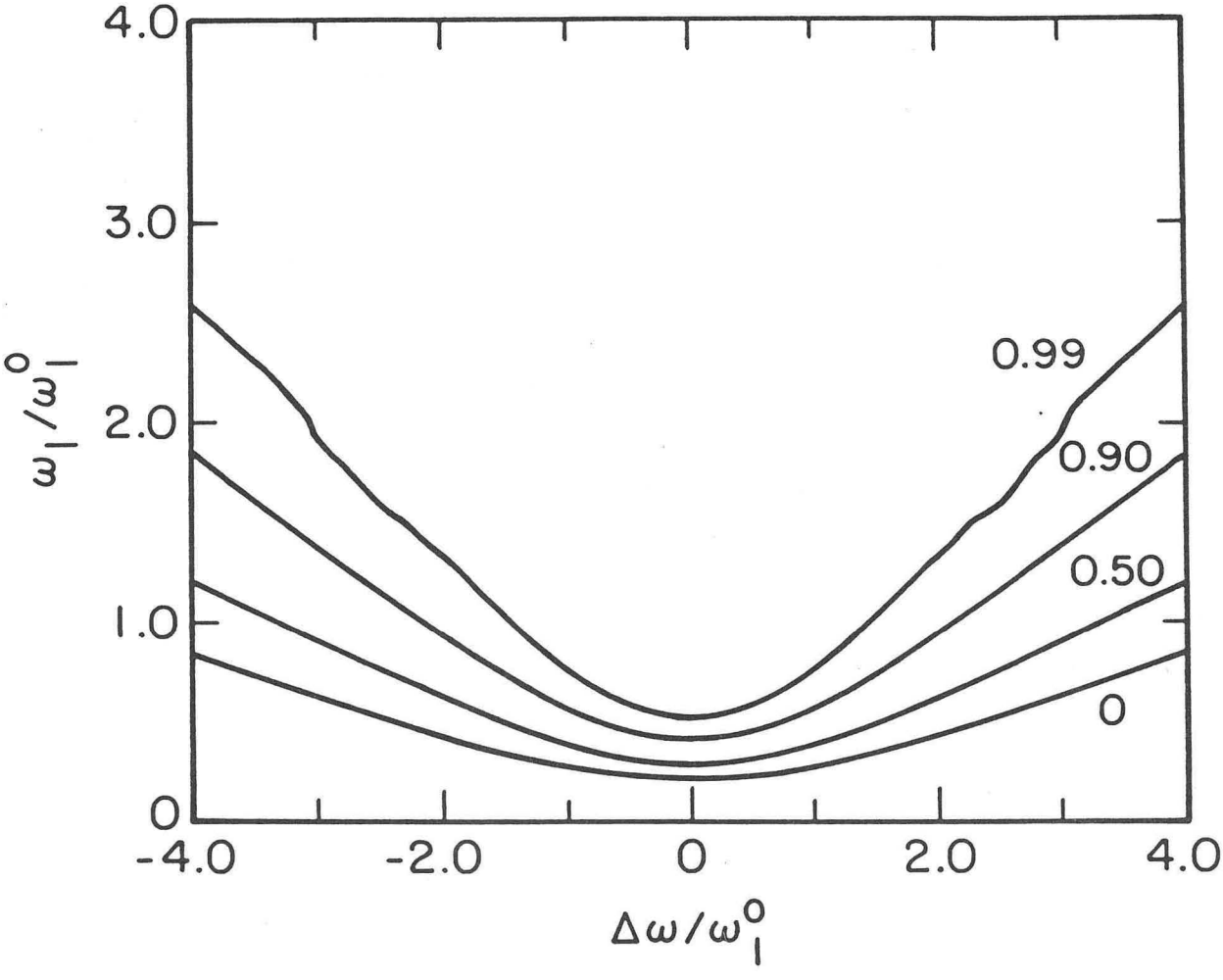

XBL 8412-5493

Figure 11

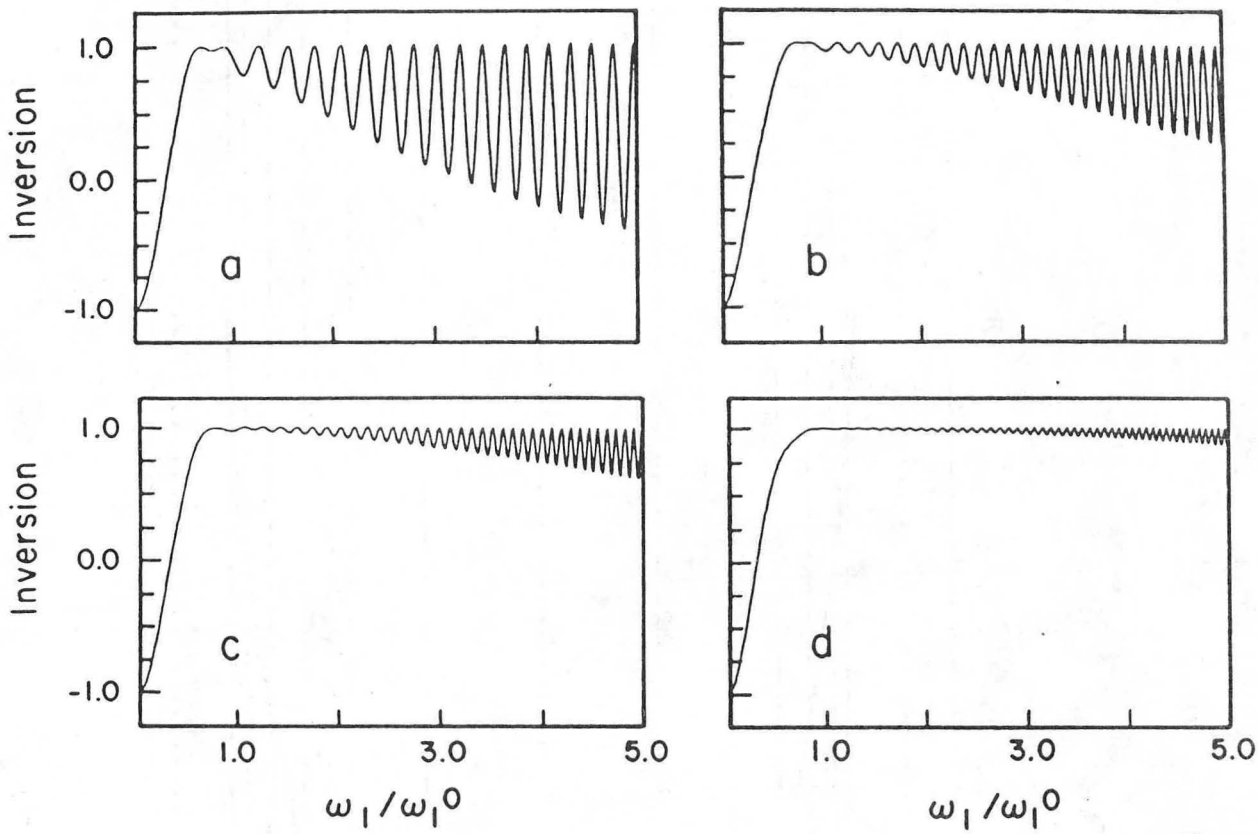

XBL 855-2603

Figure 12

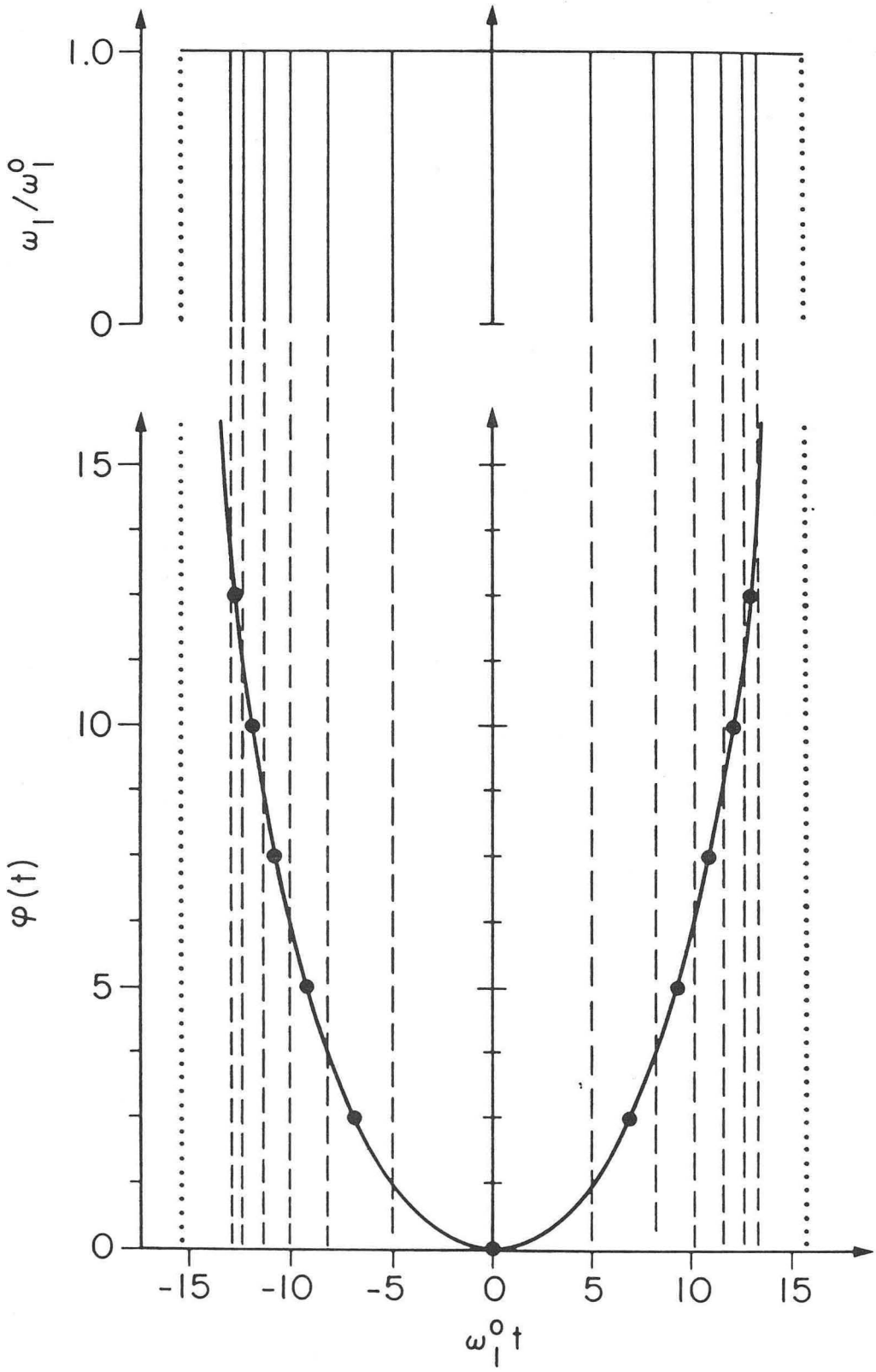

XBL 855-2616

Figure 13a

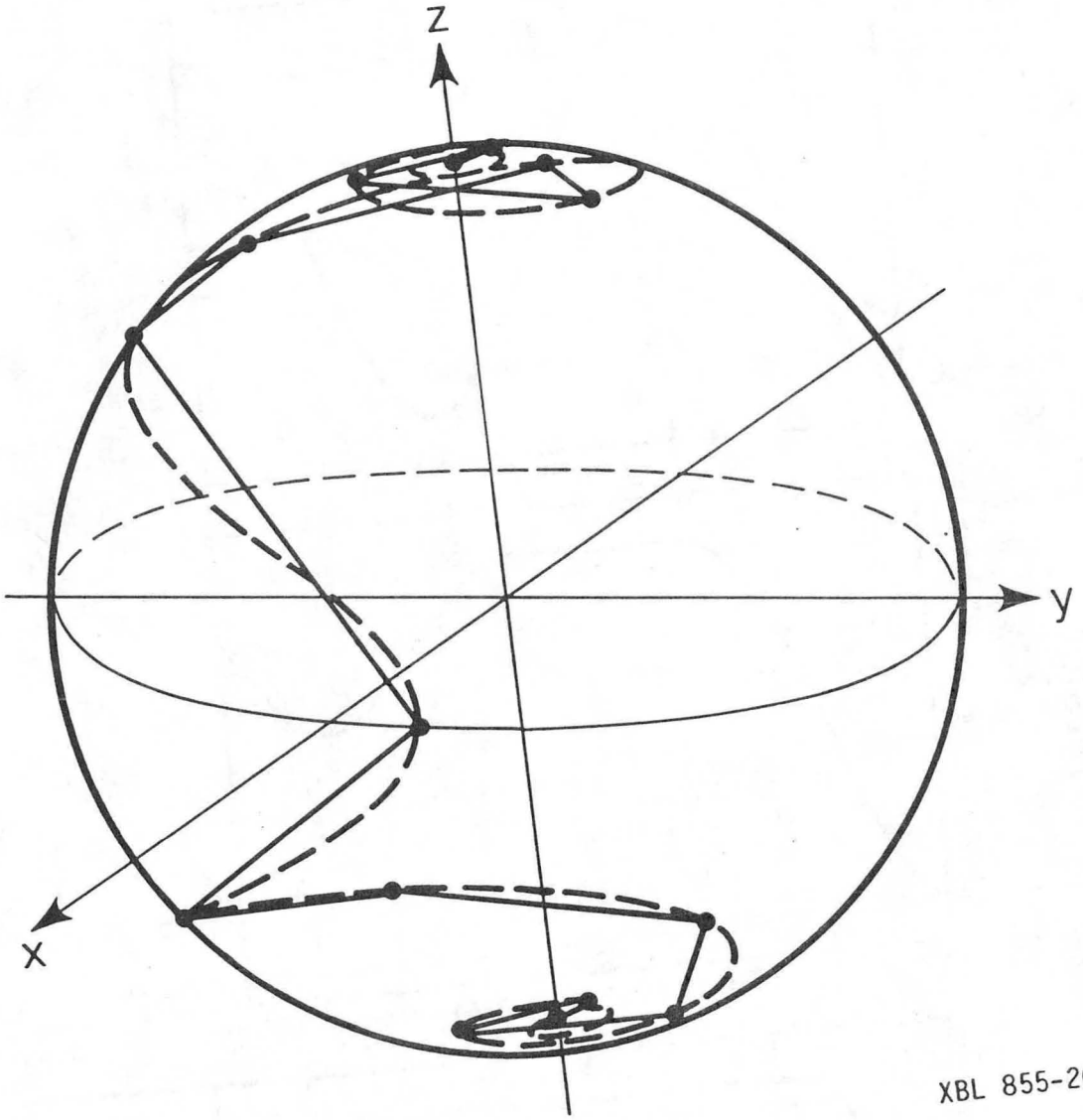

XBL 855-2642

Figure 13b

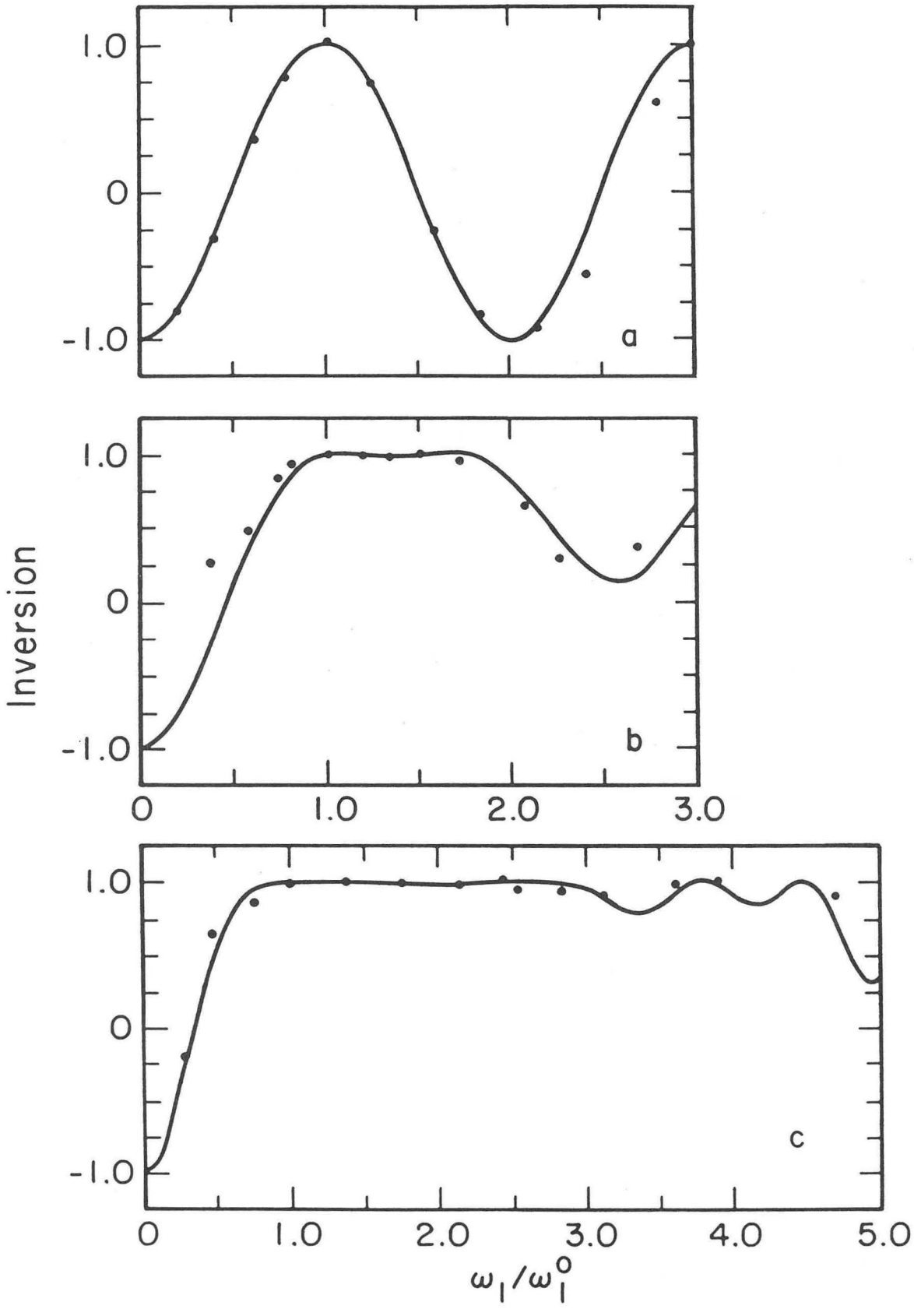

XBL 855-2607

Figure 14

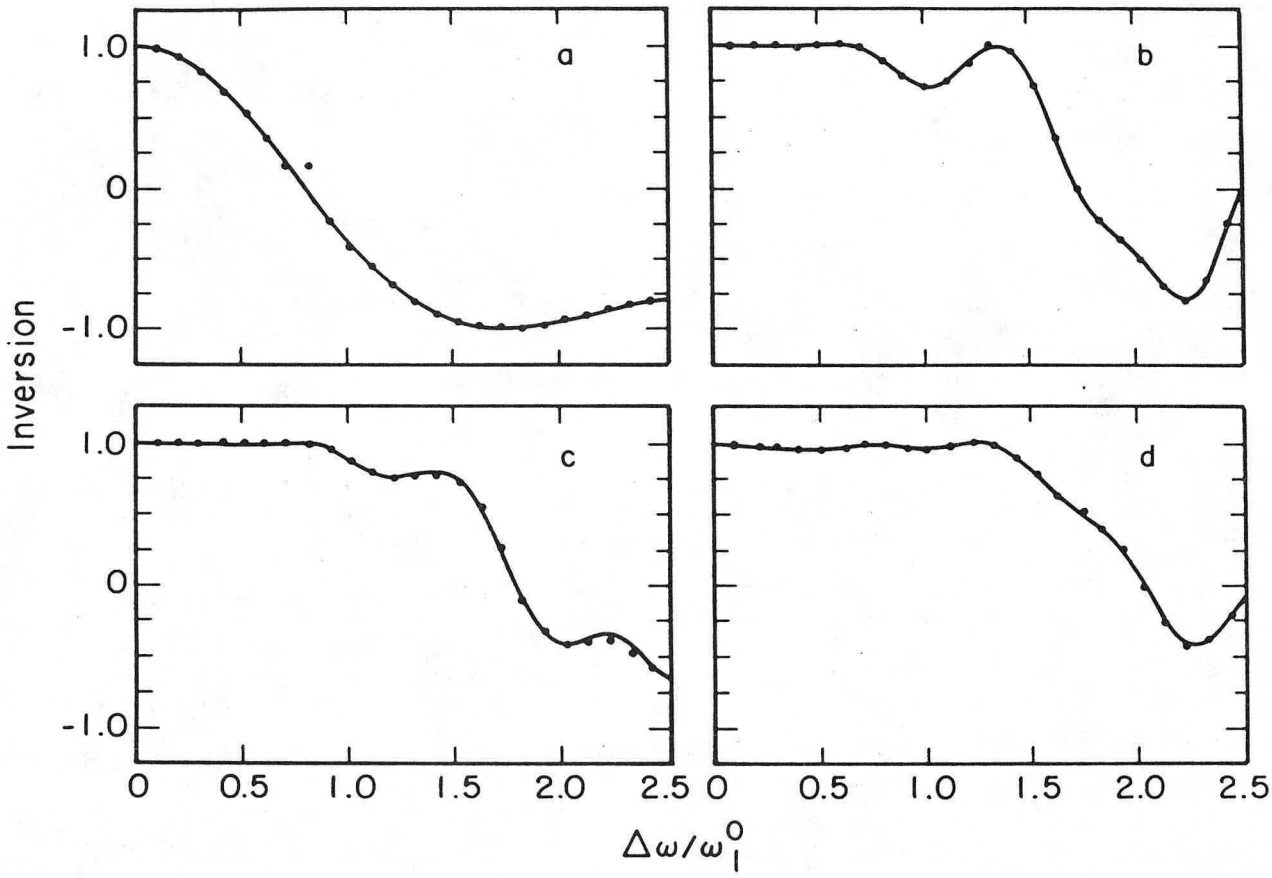

XBL 855-2606

Figure 15

This report was done with support from the Department of Energy. Any conclusions or opinions expressed in this report represent solely those of the author(s) and not necessarily those of The Regents of the University of California, the Lawrence Berkeley Laboratory or the Department of Energy.

Reference to a company or product name does not imply approval or recommendation of the product by the University of California or the U.S. Department of Energy to the exclusion of others that may be suitable.

LAWRENCE BERKELEY LABORATORY
TECHNICAL INFORMATION DEPARTMENT
UNIVERSITY OF CALIFORNIA
BERKELEY, CALIFORNIA 94720